

Controlling Enzyme Inhibition Using an Expanded Set of Genetically Encoded Amino Acids

A Thesis

Presented to
the faculty of the School of Engineering and Applied Science
University of Virginia

in partial fulfillment
of the requirements for the degree

Master of Science

by

Shun Zheng

May

2013

APPROVAL SHEET

The thesis
is submitted in partial fulfillment of the requirements
for the degree of
Master of Science

AUTHOR

The thesis has been read and approved by the examining committee:

Inchan Kwon

Advisor

John O'Connell

Roseanne Ford

Michael Shirts

Accepted for the School of Engineering and Applied Science:



Dean, School of Engineering and Applied Science

May
2013

Abstract

Enzyme inhibition plays an important role in drug development, metabolic pathway regulation, and biocatalysis with product inhibition. When an inhibitor is structurally highly similar to the substrate of an enzyme, controlling inhibitor binding without affecting substrate binding is often challenging and requires fine tuning of the active site. A carefully selected, extended set of genetically encoded amino acids is hypothesized to precisely modify the enzyme active site to reduce inhibitor binding without compromising substrate binding. To validate this hypothesis, murine dihydrofolate reductase (mDHFR), its substrate dihydrofolate (DHF), and inhibitor methotrexate (MTX) were chosen as a model system. Structural models of mDHFR variants containing non-natural amino acids (NAAs) complexed with each ligand were constructed to identify a key residue for inhibitor binding and NAAs to replace the key residue. Two mutants containing pBrF and 2Nal at position 31 (mDHFR^{pBrF31} and mDHFR^{2Nal31}) were prepared. The three mDHFR samples (mDHFR^{WT}, mDHFR^{pBrF31}, and mDHFR^{2Nal31}) were used for inhibitor binding assays and kinetic analysis. The results revealed that replacing the phenylalanine at position 31 with two phenylalanine analogs (*p*-bromophenylalanine (pBrF) and *L*-2-naphthylalanine (2Nal)) enhanced binding affinity toward the substrate DHF over the inhibitor MTX by 3.9 and 5.6 times, respectively. Such an enhanced selectivity was mainly due to a reduced inhibitor binding affinity by 2.1±1.1 and 4.3±2.0 times, respectively. The catalytic efficiency of the mDHFR variant containing pBrF was comparable to that of wild-type mDHFR, whereas the mDHFR variant containing 2Nal exhibited a moderate decrease in the catalytic efficiency. The work described here clearly demonstrated the feasibility of selectively controlling enzyme inhibition using an expanded set of genetically encoded amino acids.

Acknowledgements

I would like to thank the following people:

My research advisor Professor Inchan Kwon for his continuing guidance and insight.

Professor John O'Connell, Professor Michael Shirts, and Professor Roseanne Ford for serving on my committee.

I thank my labmates from Kwon group for their assistance and advice, particularly Edward Wong, Simpson Gregoire, Jacob Irwin, and Sungin Im.

I also wish to thank all my friends, whether around me or not, for their encouragement and advice.

My deepest gratitude goes to my family - my parents, my brother, and sister-in-law, as well as their son and my dear nephew - for their altruistic love and support.

Finally, this thesis is dedicated to the loving memory of my grandfather (1925-2012), who has always reminded me of being an upright and responsible person.

Table of contents

Abstract	i
Acknowledgements	ii
Table of Contents	iii
List of Figures	iv
List of Tables	vii
List of Abbreviations and Symbols	viii
Chapter 1. Background	1
1.1. Enzyme	1
1.2. Enzyme Inhibition	2
1.3. Non-natural Amino Acids in Protein Engineering	3
1.4. Non-natural Amino Acids in Enzyme Engineering	8
Chapter 2. Introduction	11
2.1. Model System	11
2.2. Research Scope and Objective	12
Chapter 3. Analysis of DHFR Structures	13
3.1. Crystal Structures from Protein Data Bank	13
3.2. Finding the Key Residue in the Active Site of mDHFR	15
3.3. Non-natural Amino Acid Mutagenesis <i>in silico</i>	17
Chapter 4. Preparation of Three mDHFR Samples	20
4.1. Theory	20
4.2. Materials and Methods	25
4.3. Results and Discussion	29
4.3.1. Expression of mDHFR ^{WT} , mDHFR ^{pBrF31} , and mDHFR ^{2Nal31}	29
4.3.2. Purification of mDHFR ^{WT} , mDHFR ^{pBrF31} , and mDHFR ^{2Nal31}	30
4.3.3. MALDI-TOF MS for Confirmation of pBrF and 2Nal Incorporation	33
Chapter 5. Controlling Enzyme Inhibition with Non-natural Amino Acids	35
5.1. Theory	35
5.1.1. Determination of Dissociation Constant	35
5.1.2. Determination of Michaelis Constant	36
5.2. Materials and Methods	37
5.3. Results and Discussion	38
5.3.1. Binding Affinity with Inhibitor MTX	38
5.3.2. Binding Affinity with Substrate DHF	40
Chapter 6. Conclusions	44
References	45

List of Figures

Figure 1.1. Two distinct, but complementary strategies have been developed for the incorporation of NAAs into proteins in *E. coli*. Residue-specific incorporation is achieved by globally replacing one natural amino acid with one NAA using endogenous protein synthesis machinery in *E. coli*, which usually leads to incorporation of a NAA at multiple sites of a target protein. Site-specific incorporation is achieved by suppression of one stop codon using heterologous orthogonal pair of tRNA/aaRS specific for a NAA, which usually results in incorporation of a NAA at single site of a target protein. Both residue- and site-specific incorporation have been used to improve enzyme properties, such as activity and stability. If residue-specific incorporation improves one enzyme property but causes loss of other enzyme properties, direction evolution can be applied to recapitulate the lost enzyme properties.5

Figure 1.2. Two strategies to reduce the loss of enzyme stability and/or activity upon residue-specific incorporation of NAAs. (A) Stepwise increase of stability/activity using directed evolution; (B) Stepwise increase of stability/activity using variants with high folding robustness.6

Figure 2.1. Conversion of DHF into THF catalyzed by DHFR in the presence of NADPH. Portions of the chemical structure of the mDHFR inhibitor MTX that differ from DHF are circled.11

Figure 3.1. Sequence and structure alignment of mDHFR and hDHFR. (A) Sequence alignment of mDHFR and hDHFR. F31 is highlighted as bold and mismatching residues as red. (B) Structure alignment of mDHFR and hDHFR, shown is the enlarged view of the active site. Blue: mDHFR; Gray: hDHFR; Red: MTX bound to mDHFR; Purple: MTX bound to hDHFR. Phe31 and MTX are shown as sticks. (C) Structure alignment of mDHFR and hDHFR. Blue: mDHFR; Gray: hDHFR; Red: MTX; Yellow: NADPH. Figures are drawn with PyMOL.14

Figure 3.2. Multiple sequence alignment of mammalian DHFRs. The amino acid sequences obtained from five different mammals (mouse, rat, human, monkey, and cattle) were aligned (: = conserved residues; = semi-conserved residues; * = strictly conserved residues).16

Figure 3.3. Chemical structure of substrate DHF and inhibitor MTX. MTX is a competitive inhibitor for mDHFR whose structure is similar to DHF.16

Figure 3.4. Interactions of key residues in the active site of hDHFR^{WT} with MTX or FOL (Figures from PDB). (A) hDHFR^{WT}:MTX; (B) hDHFR^{WT}:FOL. Black dashed line: hydrogen bonds, salt bridges, metal interactions; Green solid line: hydrophobic interactions; Green dashed line: π - π , π -cation interactions. 17

Figure 3.5. Chemical structure of phenylalanine (Phe), *p*-bromophenylalanine (pBrF), and L-2-naphthylalanine (2Nal). 18

Figure 3.6. Structural models of mDHFR:ligand complexes. Variants with F31 are real crystal structures obtained from PDB, while variants with pBrF31 or 2Nal31 are constructed structural models. The crystal structure of hDHFR^{WT}:inhibitor (PDB ID: 1U72) (*top left*); the structural model of mDHFR^{pBrF31}:inhibitor (*top middle*) and mDHFR^{2Nal31}:inhibitor complex (*top right*). The structural models of mDHFR^{WT}:substrate (wild-type human DHFR:folate complex; PDB ID:2W3M) (*bottom left*); mDHFR^{pBrF31}:substrate (*bottom middle*) and mDHFR^{2Nal31}:substrate (*bottom right*). Inhibitor (orange); substrate (bright orange); carbon atom in side chain (magenta); bromine atom in side chain (light pink). 19

Figure 4.1. Schematic diagram for the preparation of mDHFR variants. 20

Figure 4.2. Translation process in *E. coli*. 21

Figure 4.3. Crystal structure of mDHFR (PDB ID: 1U70, shown as cartoon) complexed with MTX (red) and NADPH (yellow). (A) Front view showing bound MTX and NADPH. (B) Side view, N-terminus was shown as green and C-terminus as orange. 23

Figure 4.4. Binding of 6xHis tag with Ni-NTA matrix. 24

Figure 4.5. SDS-PAGE data for the confirmation of the expression of mDHFR^{WT}, mDHFR^{pBrF31}, and mDHFR^{2Nal31}. Lane 1: marker, the size of each band is shown on the left; Lane 2: cells for mDHFR^{WT} expression, before induction; Lane 3: cells expressing mDHFR^{WT}, after induction; Lane 4: cells for mDHFR^{pBrF31} expression, before induction; Lane 5: cells expressing mDHFR^{pBrF31}, after induction; Lane 6: cells for mDHFR^{2Nal31} expression, before induction; Lane 7: cells expressing mDHFR^{2Nal31}, after induction. 30

Figure 4.6. SDS-PAGE data for soluble and insoluble portion of cells expressing mDHFR^{WT} and mDHFR^{pBrF31}. (A) mDHFR^{WT}. Lane 1: marker, the size of each band was shown on the left; Lane 2: soluble portion; Lane 3: insoluble portion. (B) mDHFR^{pBrF31}. Lane 1: marker, the size of each band was shown on the left; Lane 2: soluble portion; Lane 3: insoluble portion. mDHFR variants were indicated with arrow. 32

Figure 4.7. SDS-PAGE of purified mDHFR variants. Lane 1: maker, the size of each band was shown on the left; Lane 2: mDHFR^{WT}; Lane 3: mDHFR^{pBrF31}; Lane 4: mDHFR^{2Nal31}.32

Figure 4.8. Incorporation of pBrF and 2Nal at mDHFR position 31 confirmed by MALDI-TOF MS of tryptic digests of mDHFR variants. Peptide_F31 refers to a tryptic fragment of mDHFR^{WT} (residues 18-32; NGDLPWPPLRNEAFK). Peptide_pBrF31 and Peptide_2Nal31 refer to the form of the peptides containing pBrF and 2Nal in place of Phe at position 31, respectively. See text for details.34

Figure 5.1. Linear relationship between tryptophan fluorescence and mDHFR^{WT} concentration. ($R^2=0.9978$; $n=3$).40

Figure 5.2. Tryptophan fluorescence spectra of the mDHFR samples in the presence of MTX. The tryptophan fluorescence of three mDHFR variants (WT: mDHFR^{WT}; pBrF: mDHFR^{pBrF31}; 2Nal: mDHFR^{2Nal31}) were quenched in the presence of 1.0×10^4 nM of MTX.40

Figure 5.3. The fraction of mDHFR variants quenched (Q) at varying concentrations of MTX. WT: mDHFR^{WT}; pBrF31: mDHFR^{pBrF31}; 2Nal31: mDHFR^{2Nal31}. MTX concentration ranged from 0 to 1.0×10^6 nM. The data were fitted into a curve to determine K_D values using Eqn. 5.1.41

Figure 5.4. Comparison of reaction rate for three mDHFR variants. WT: mDHFR^{WT}; pBrF: mDHFR^{pBrF31}; 2Nal: mDHFR^{2Nal31}. Reaction was performed with 30 μ M of DHF and 60 μ M of NADPH dissolved in MTEN buffer.43

Figure 5.5. Enzyme reaction rate (μ M of DHF consumed by per μ M of enzyme per minute) at various concentrations of DHF. WT: mDHFR^{WT}; pBrF31: mDHFR^{pBrF31}; 2Nal31: mDHFR^{2Nal31}. DHF concentration ranged from 1 to 50 μ M ($n=3\sim 5$). The data were fitted into a curve to determine K_M and k_{cat} values using Eqn. 5.2.43

List of Tables

Table 5.1. Symbols and their physical meanings.	35
Table 5.2. MTX dissociation constants and kinetic parameters of mDHFR variants.	44

List of Abbreviations and Symbols

aaRS	aminoacyl-tRNA synthetase
AFWK	a phenylalanine/tryptophan/lysine auxotrophic <i>Escherichia coli</i> strain
ATP-PPi	adenosine triphosphate-pyrophosphate
BSA	bovine serum albumin
DHB	2,5-dihydroxybenzoic acid
DHFR	dihydrofolate reductase
DHF	dihydrofolate
<i>E. coli</i>	<i>Escherichia coli</i>
FOL	folate
F31	phenylalanine at position 31
GFP	green fluorescent protein
hDHFR	human dihydrofolate reductase
hDHFR ^{WT}	wild-type human dihydrofolate reductase
hDHFR ^{pBrF31}	human dihydrofolate reductase with pBrF at position 31
hDHFR ^{2Nal31}	human dihydrofolate reductase with 2Nal at position 31
LB	Luria-Broth
IPTG	isopropyl-β-D-thiogalactopyranoside
MAD	multiple wavelength anomalous diffraction
MALDI-TOF	matrix-assisted laser desorption-ionization time-of-flight
MS	mass spectrometry
mDHFR	murine dihydrofolate reductase
mDHFR ^{WT}	wild-type murine dihydrofolate reductase
mDHFR ^{pBrF31}	murine dihydrofolate reductase with pBrF at position 31
mDHFR ^{2Nal31}	murine dihydrofolate reductase with 2Nal at position 31
mRNA	messenger RNA
MTX	methotrexate
NAA	non-natural amino acid
NADPH	nicotinamide adenine dinucleotide phosphate

Ni-NTA	nickel-nitrilotriacetic acid
NMR	nuclear magnetic resonance
OD	optical density
pBrF	<i>p</i> -bromophenylalanine
pBrF31	<i>p</i> -bromophenylalanine at position 31
Phe	phenylalanine
PPi	sodium pyrophosphate
RINA	residue-specific incorporation of non-natural amino acid
SAD	single wavelength anomalous diffraction
SDS-PAGE	sodium dodecyl sulfate polyacrylamide gel electrophoresis
SINA	site-specific incorporation of non-natural amino acid
TFA	trifluoroacetic acid
THF	tetrohydrofolate
tRNA	transfer RNA
yPheRS	yeast phenylalanyl-tRNA synthetase
2Nal	<i>L</i> -2-naphthylalanine
2Nal31	<i>L</i> -2-naphthylalanine at position 31
6xHis	six histidine-tag
<i>E</i>	enzyme
<i>M</i>	methotrexate
<i>EM</i>	enzyme-MTX complex
<i>S</i>	substrate
<i>ES</i>	enzyme-substrate complex
<i>P</i>	product
K_D	dissociation constant
$[E]_0$	initial concentration of enzyme
$[E]$	concentration of free enzyme
$[M]_0$	initial concentration of MTX
$[M]$	concentration of free MTX

$[EM]$	concentration of enzyme-MTX complex
Q	quenched fraction of enzyme
K_M	Michaelis constant
k_{cat}	turnover rate
$[S]$	concentration of free DHF
$[ES]$	concentration of enzyme-DHF complex
$[P]$	concentration of THF
k_{cat}/K_M	catalytic efficiency

1. Background

1.1. Enzyme

Enzymes are proteins catalyzing chemical reactions with high efficiency and specificity. In nature, enzymes are synthesized by living organisms and are involved in tremendously diverse metabolic reactions throughout their lives. The excellent catalytic activity, together with milder working environment compared with the traditional chemical reactions frequently requiring extreme temperature or pressure, has led enzymes to their broad applications in basic science as well as in the industrial processes [1].

The first industrial use of enzyme dated back to the year 1913 when the German chemist Otto Röhm discovered that pancreatic trypsin could remove proteinaceous stains from clothes. Since then, enzymes have experienced several technological innovations to reach the current industrially proven level usages [2–4]. The first stage was the era of “traditional biocatalysis” about a century ago, in which natural enzymatic reactions were used as their original shape in nature, involving the use of natural enzymes to produce natural products with natural substrates. An example can be given by the conversion of glucose to fructose with glucose isomerase [5]. Following that was the era of “broad-substrate-range biocatalysis” in the 1980s and 1990s, which involved the modification of the components of the enzymatic reactions. This was still the use of natural reactions or pathways and can be exemplified by the manufacture of pharmaceutical intermediates using lipases [6]. The third era occurred in the late 1990s, marked by the use of non-natural reactions and pathways with enzymes engineered by advanced modern biotechnologies like recombinant DNA technology and direct evolution. Examples include hydrolases and a few ketoreductases in the industrial scale [7].

Currently, enzymes are widely employed in diverse fields, such as their technical uses in the pulp and paper industry, and the textile industry; uses in food processing like dairy industry, baking industry, brewing industry and starch processing; uses in animal feeds industry; uses in organic synthesis industry; uses in cosmetics industry, and finally in the pharmaceutical industry [8–11]. According to a research report from Austrian Federal Environment Agency, about 64 enzymes were used in technical application, about 158 enzymes were used in food industry, and about 57 enzymes were used in feed industry [12]. The global enzymes market is estimated to rise 7 percent to \$4.4 billion in 2015 [13].

1.2. Enzyme Inhibition

Despite the broad and well-established commercial uses, enzymes in production processes often suffer from weak efficiency during the catalytic processes, due to the harsh conditions in the real practice and sometimes the substrate and product inhibition. Hydrolysis of lactose by β -galactosidase is a promising process in the food industry to prepare lactose-free products for the great percentage of population with lactose intolerance over the world (70%) [14,15]. However, it was shown by several studies that β -galactosidase was competitively inhibited by its catalytic product galactose. The currently employed cellulolytic enzyme systems including the widely studied *Trichoderma reesei* enzymes, convert the lignocellulosic biomass to liquid fuels and other valuable products. The significant inhibition of the enzymes by the products cellobiose and glucose is particularly problematic in large-scale processing of cellulosic biomass where the cost accounts for a significant parameter [16].

Besides the issues in real industrial production process, inhibition of enzyme has also been an important topic for understanding the molecular mechanism of enzymatic reaction, regulating metabolic pathway, and developing enzyme-inhibitor pharmaceuticals [17–20]. Most drugs in

clinical use are enzyme inhibitors; most antibiotic-resistant pathogenic bacteria variants have mutations in enzymes. Modulating enzyme susceptibility to inhibitors is also an emerging research area in synthetic biology [18]. Therefore, there is a great incentive to control the interaction of the enzymes with their inhibitors that come in diverse forms. Recent advancement in the experimental and computational protein/enzyme engineering provides valuable tools for the improvement of the original traits of enzymes as well as the development of novel enzymes.

1.3. Non-natural Amino Acids in Protein Engineering

As enzymes are proteins, all protein engineering techniques developed to date are applicable in the engineering of enzymes.

Expanding protein sequence space is critical in the success of protein engineering [21]. Therefore, diverse techniques, such as site-directed mutagenesis, directed evolution, insertional/deletional engineering, circular permutation, and de novo protein design, have been developed to expand the space of amino acid sequence, leading to an increased pool of available proteins [22–27].

Despite the tremendous forms of sequences and structures, these proteins, however, with extremely few exceptions [28–30], are composed of surprisingly limited 20 kinds of amino acids (natural amino acids). Those proteins, as the ultimate results of natural evolution so far, might be sufficient for nature, but sometimes not as satisfactory for scientists and engineers. The advent of the techniques of incorporating non-natural amino acids (NAAs) into proteins in recent years greatly intrigued people's interest in this area. Incorporation of NAAs holds great promise in generating proteins with novel or improved properties that cannot be offered by natural amino acids [31–34]. Unlike the play of limited number of amino acid species as the traditional

techniques, this implies the possibilities of creating novel molecules that might have been bypassed or never existed in nature during the long term evolutionary progress.

Ever since the discovery of naturally occurring NAA in the living organisms [28–30], scientists have been investing great efforts to develop techniques to incorporate various NAAs into proteins. In terms of the consequence of NAA incorporation, it can be generally categorized into two groups: residue- and site- specific incorporation (RINA and SINA), and in many ways they are complementary to each other (Fig. 1.1). RINA achieves global replacement of one natural amino acid with its analog throughout a target protein amino acid sequence using an *auxotrophic Escherichia coli* (*E. coli*) strain, which lacks the ability to biosynthesize a natural amino acid(s) [35,36]. Despite successful cases of applications [34,37], RINA is limited in improving protein properties due to the potential risk of over-perturbation of the original protein structure and activity caused by the incorporation of NAAs at non-permissive sites of proteins [38–41]. This can be alleviated or avoided by carefully choosing the NAAs as well as the sites to incorporate in the target protein beforehand [42–44]. Alternative strategies include the recovery of the attenuated activity or stability of the functional proteins upon NAA incorporation with directed evolution thereafter, and starting with candidates with higher folding robustness [45–47]. (Fig. 1.2)

In contrast to the RINA, SINA can generate mutants with minimal perturbation of the structure thus is unrivaled for precise control of protein structures and activities. Technically, a variety of methods for site-specific incorporation have been developed, including the chemical and biological synthesis. In biosynthetic methods, the cellular machinery of the living cell to synthesize proteins (Fig. 1.1) is harnessed to incorporate NAAs and this can be conducted both *in vitro* and *in vivo*. For the case of *in vitro*, the truncated tRNAs are enzymatically ligated to

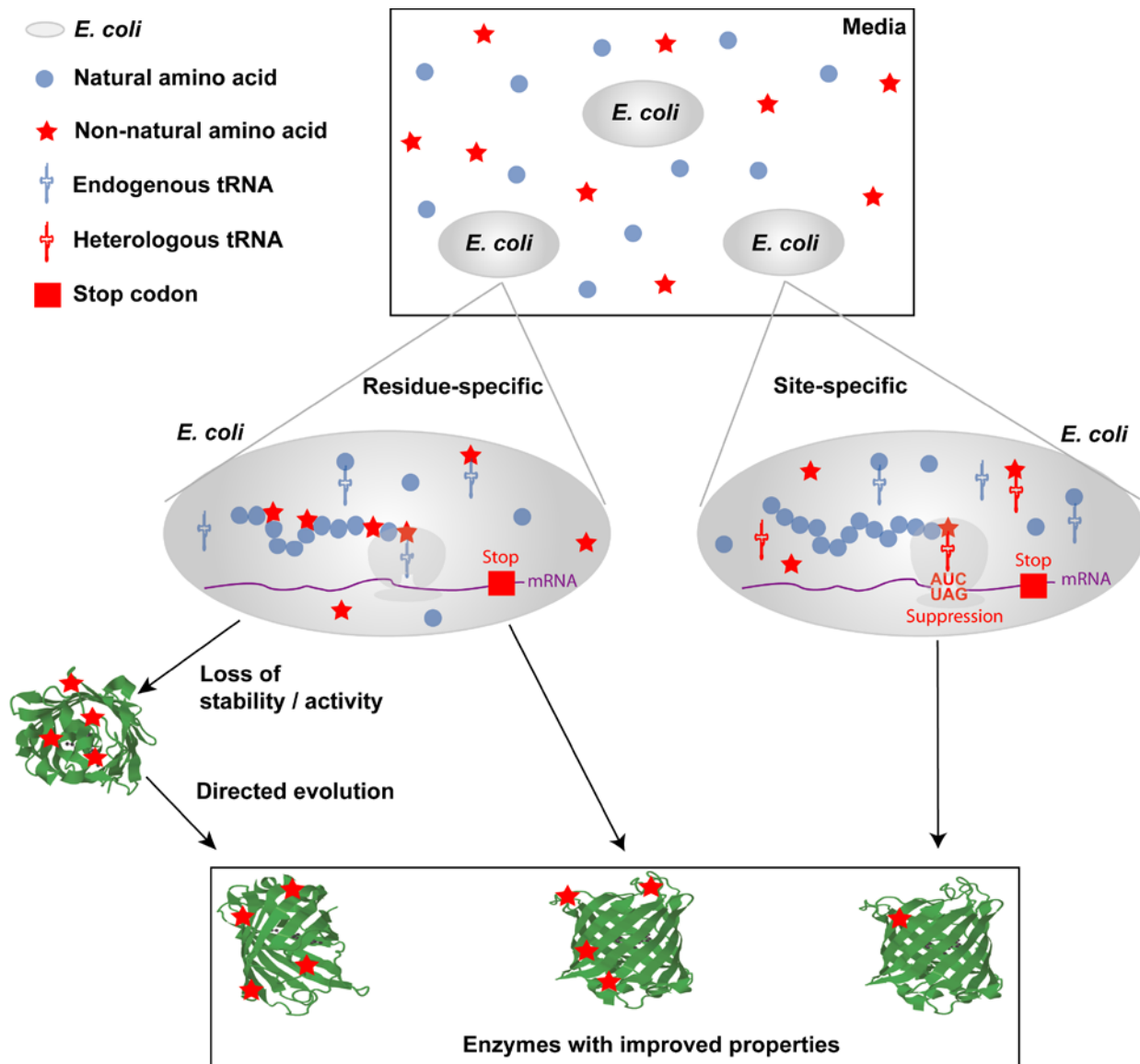


Figure 1.1. Two distinct, but complementary strategies have been developed for the incorporation of NAAs into proteins *in E. coli*. Residue-specific incorporation is achieved by globally replacing one natural amino acid with one NAA using endogenous protein synthesis machinery in *E. coli*, which usually leads to incorporation of a NAA at multiple sites of a target protein. Site-specific incorporation is achieved by suppression of one stop codon using heterologous orthogonal pair of tRNA/aaRS specific for a NAA, which usually results in incorporation of a NAA at single site of a target protein. Both residue- and site-specific incorporation have been used to improve enzyme properties, such as activity and stability. If residue-specific incorporation improves one enzyme property but causes loss of other enzyme properties, direction evolution can be applied to recapitulate the lost enzyme properties.

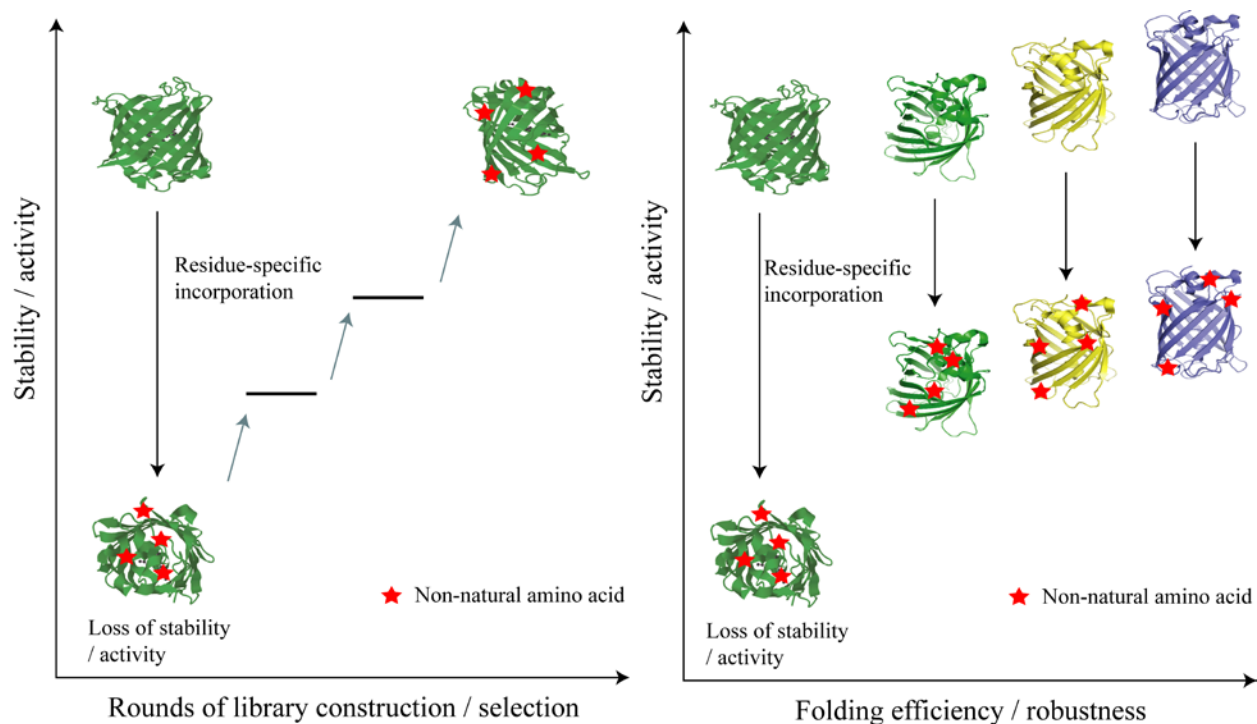


Figure 1.2. Two strategies to reduce the loss of enzyme stability and/or activity upon residue-specific incorporation of NAAs. (A) Stepwise increase of stability/activity using directed evolution; (B) Stepwise increase of stability/activity using variants with high folding robustness.

chemically aminoacylated nucleotides that carries NAAs and then cell-free translation system uses them to incorporate the attached NAAs into the target protein. A variation of this is the injection or transfection of those tRNAs into living cells and the translation process subsequently occurs inside the cell [48,49]. A more elegant and simpler way would be the SINA into a protein *in vivo*. This method incorporates an NAA into a site(s) of a target protein using cells equipped with a heterologous orthogonal pair of suppressor tRNA/aminoacyl-tRNA synthetase (aaRSs) specific for the NAA. Provided with NAAs in the media, the cells automatically uptake and incorporate them into the designated position of the protein by use of this imported pathway. So

far over a hundred NAAs, including serine, lysine, leucine, valine, proline, tyrosine, phenylalanine, and tryptophan analogs have been introduced into a protein in *E. coli*, yeast, or mammalian cells [31,33,34].

To date, most applications of NAA incorporation techniques have focused on providing a target protein with a new functionality that cannot be obtained with natural amino acids, which is demonstrated in the following fields. First, incorporation of a NAA containing a reactive functional group, such as *p*-azidophenylalanine (pN₃F) or *p*-acetylphenylalanine, provides new chemical reactivity to proteins. Incorporation of pN₃F to protein-based biomaterials allows photocross-linking of the biomaterials on the surface for the further application in biosensor [50]. Incorporation of *p*-acetylphenylalanine at a specific site in human growth hormone achieves site-specific conjugation of polyethylene glycol to human growth hormone, leading to favorable pharmacodynamic properties in animal tests [51]. Second, a NAA in a protein can serve as a probe of protein folding, protein–protein interactions, and ligand binding to proteins. The nitrile group of *p*-cyanophenylalanine has been used as a fluorescence and infrared probe to study ligand binding to myoglobin, folding of ribosomal protein L9, and aggregation of islet amyloid polypeptide [52–54]. Incorporating NAA can also facilitate NMR spectroscopic studies of proteins [52–55]. In particular, labeling a protein with a NAA containing a ¹⁹F atom is a popular method to characterize protein structural changes by NMR spectroscopy [56–60]. Third, NAAs containing a heavy atom, such as selenium, bromine, or iodine, are widely used to facilitate the resolution of X-ray crystal structures of proteins [61–64]. Residue-specific incorporation of selenomethionine into proteins using a methionine auxotrophic *E. coli* strain allows the determination of X-ray crystallographic structures of proteins by multiple (MAD) or single wavelength anomalous diffraction (SAD) [65,66]. Site-specific incorporation of *p*-

iodophenylalanine and 3-iodotyrosine into bacteriophage T4 lysozyme and *N*-acetyltransferase, has also been reported to facilitate the SAD phasing [63,64]. Fourth, NAA has been used to modulate the spectral property of the proteins, such as fluorescence [67,68]. The spectral property of the green fluorescent protein (GFP) changes according to the composition of its chromophore. Schultz et al. replaced Tyr66 residue in the chromophore of GFP with one of five Phe analogs, *p*-aminophenylalanine, *p*-methoxyphenylalanine, *p*-iodophenylalanine, *p*-bromophenylalanine, and *L*-3-(2-naphthyl)alanine [67]. The wavelengths for both absorbance and emission maxima increase according to the electron-donating ability of the side chain of NAA. Kwon et al. replaced Trp66 in the chromophore of a cyan fluorescent protein with 6-chlorotryptophan, 6-bromotryptophan, 5-bromotryptophan, and benzothienylalanine, and all of the resulting variants caused blue shifts in the fluorescence emission and absorption maxima [68].

Nowadays, the main technical theme in this area is the endeavor for the improvement of the incorporation fidelity, simultaneous incorporation of multiple NAAs, the increase of the yield as well as the expansion of NAA to incorporate, and it is believed that this technology has been ready for the exploration of its applications in broader areas, among which the improvement of enzyme will take a good portion [32–34].

1.4. Non-natural Amino Acids in Enzyme Engineering

The numerous applications of NAAs have been studied widely as discussed in last section. However, their applications in the area of enzyme engineering have not been explored as much, though this is a hot biotechnology topic due to society's increased interest in environmentally friendly chemistry as well as issues preventing applications of specific enzymes in the industry. Both *in vivo* RINA and SINA have been attempted for the modulation of enzyme properties.

Even though RINA often leads to a loss in activity of enzymes, the simplicity of this method has made it popular in the exploitation of their applications in enzyme engineering [47,58,69–81]. For example, Armstrong et al. replaced tryptophan residues of glutathione S-transferase (GST), resulting in 4-fold and 2-fold higher values of turnover number and catalytic efficiency than those of native enzyme, respectively [69]. Arnold et al replaced 13 methionine residues in the heme domain variant (TH-4) of the cytochrome P450 from *Bacillus megaterium* with a methionine analog norleucine (Nor). The activity of TH-4 with norleucine was two-fold greater than that of TH-4 (Met), with decreased thermostability [73]. Swartz et al. globally replaced Met residues of Gaussia luciferase (GLuc) by a methionine analog azidohomoalanine using cell-free protein synthesis and the resulting mutant exhibited 3-fold higher stability than wild-type GLuc [77].

Recently SINA has also been, though with limited number of cases, successfully used to improve enzyme properties. Mehl et al. reported their pioneering work to improve enzyme activity using SINA Phe124 in the active site of *E. coli* nitroreductase was replaced by eight different Phe analogs, *p*-aminophenylalanine, *L*-3-(2-naphthyl)alanine, *p*-benzoylphenylalanine, *p*-methoxyphenylalanine, *p*-aminomethylphenylalanine, *p*-methylphenylalanine, *p*-trifluoromethylphenylalanine, *p*-nitrophenylalanine (pNF). Nitroreductase mutant containing pNF at residue 124 exhibited 2- and 4-fold higher activity than the best two mutants composed of natural amino acids only [82,83]. Phosphotriesterase obtained from *Agrobacterium radiobacter* (*ar*PTE) and *Pseudomonas diminuta* (*pd*PTE) are known to catalyze the hydrolysis of toxic organophosphate phosphotriester pesticides including paraoxon [84]. Studies on the crystal structure and site-directed mutagenesis of *ar*PTE revealed that Tyr309 in the active site is critical in the binding of substrate. Very recently, Jackson et al. replaced Tyr309 in *ar*PTE with one of

two NAAs, *L*-(7-hydroxycoumarin-4-yl)ethylglycine (Hco) and *L*-(7-methylcoumarin-4-yl)ethylglycine (Mco) with the combined use of *in vitro* transcription and translation of *ar*PTE. The Hco mutant exhibited 8-fold higher turnover rate than already highly efficient wild-type *ar*PTE at pH 8.5. This finding demonstrates the feasibility of improving enzyme properties without screening large size of mutant libraries.

In summary, the use of NAAs in enzyme engineering is still in its infancy and this area is on the verge of significant growth. Among those limited case studies, both RINA and SINA have been tried and focus was put on improving enzyme activity and stability. However, many other important enzyme traits, such as enzyme inhibition, and product regio- and stereo-selectivity have not yet been explored. This study will take a pace forward to show the first time a case of controlling of enzyme inhibition by SINA together with the structure-based rational design.

2. Introduction

2.1. Model System

In view of the almost unlimited species of NAAs, SINA holds great promise in precisely modifying the enzyme to achieve the targeted traits. Herein the use of SINA for controlling enzyme inhibition was studied.

Murine dihydrofolate reductase (mDHFR) and its inhibitor methotrexate (MTX) were chosen as a model system. DHFR is a ubiquitous enzyme found in all organisms, and is the target of several important anticancer and antibiotic drugs [85]. The family of DHFRs catalyzes the conversion of dihydrofolate (DHF) into tetrahydrofolate (THF) using nicotinamide adenine dinucleotide phosphate (NADPH) as a cofactor (Fig. 2.1). MTX is a competitive inhibitor to mammalian DHFRs, and is structurally very similar to the substrate DHF. This made it very challenging to decrease the affinity with MTX while maintaining the affinity with DHF.

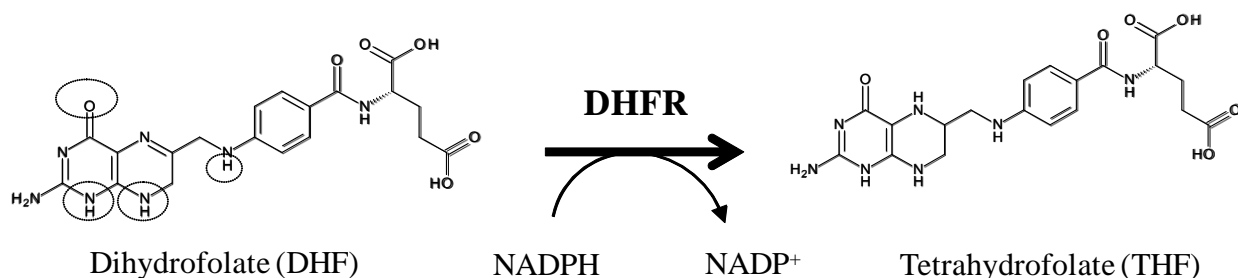


Figure 2.1. Conversion of DHF into THF catalyzed by DHFR in the presence of NADPH. Portions of the chemical structure of the mDHFR inhibitor MTX that differ from DHF are circled.

As a model system, DHFR and MTX have several favorable features. First, MTX was developed for chemotherapy by inhibiting human DHFR activity. Therefore, inhibiting DHFR

activities is a very active research area [86–89]. Second, the crystal structures of DHFRs bound to their inhibitors and substrates are readily available facilitating the identification of key residues for the inhibitor and substrate binding [86–88,90]. Third, the expression and purification of DHFRs in *E. coli* are well established [68], [91]. Fourth, kinetic assay and inhibitor binding assay for DHFRs are also well established [92,93]. Fifth, it was successfully demonstrated that several phenylalanine and tryptophan analogs can be introduced into mDHFR in a site-specific manner in *E. coli* [68], [91].

2.2. Research Scope and Objective

The overall goal of this study is to investigate the use of SINA combined with structure-based rational design to decrease the binding affinity of an enzyme mDHFR to its inhibitor without compromising the binding affinity to its substrate DHF, by carefully choosing NAAs to replace a key residue in the active site of mDHFR. To achieve the overall goal, the following research objectives were defined:

1. Search the key residue in the active site of mDHFR based on crystal structures and structural models, and choose appropriate NAAs.
2. Prepare wild-type mDHFR and site-specifically incorporate NAAs into mDHFR in *E. coli*.
3. Purify active mDHFR variants in their native forms.
4. Measure and compare the affinity of mDHFR variants with the inhibitor MTX and substrate DHF.

3. Analysis of DHFR crystal structures

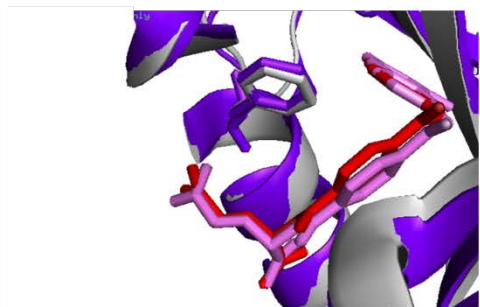
3.1. Crystal structures from Protein Data Bank

Regarding the inhibitor MTX, substrate DHF, and mDHFR, the available crystal structure is mDHFR L22R mutant complexed with MTX and NADPH (PDB ID: 1U70). Those of the wild-type mDHFR:MTX or wild-type mDHFR: dihydrofolate complex have not been resolved yet. Human DHFR (hDHFR) has greater than 95% of amino acid sequence similarity as well as structural similarity with mDHFR (Fig. 3.1). Fig. 3.1.C is the view of the alignment of the crystal structure of mDHFR^{L22R} complexed with MTX and NADPH with that of hDHFR^{WT} complexed with MTX and NADPH (PDB ID: 1U72) [86], showing that the structures almost overlap to each other. Fig. 3.1.B is a closer view of the active site. There is negligible difference in the position as well as the direction of F31 and MTX in the two crystal structures. Thus, the highly homologous hDHFR complexed with MTX or folate (FOL) which is isosteric to dihydrofolate (PDB ID: 2W3M) was used as a template to construct the structural models.

A.

<i>Mouse</i>	VRPLN CIVAV SQNMG IGKNG DLPWP PLRNE FKYFQ RMTTT SSVEG KQNLV
<i>Human</i>	V G SLN CIVAV SQNMG IGKNG DLPWP PLRNE F R Y FQ RMTTT SSVEG KQNLV
<i>Mouse</i>	IMGRK TWFSI PEKNR PLKDR INIVL SRELK EPPRG AHFLA KSLDD ALRLI
<i>Human</i>	IM G KK TWFSI PEKNR PL K GR IN L VL SRELK EPP Q G AH F LS R SLDD AL K LT
<i>Mouse</i>	EQPEL ASKVD MVWIV GGSSV YQEAM NQPGH LRLFV TRIMQ EFESD TFFPE
<i>Human</i>	EQPEL AN K VD MVWIV GGSSV Y K EAM N H PGH L KLFV TRIMQ D FESD TFFPE
<i>Mouse</i>	IDLGK YKLLP EYPGV LSEVQ EEKGI KYKFE VYEKK D
<i>Human</i>	ID L E K YKLLP EYPGV L S D VQ EEKGI KYKFE VYE K N D

B.



C.

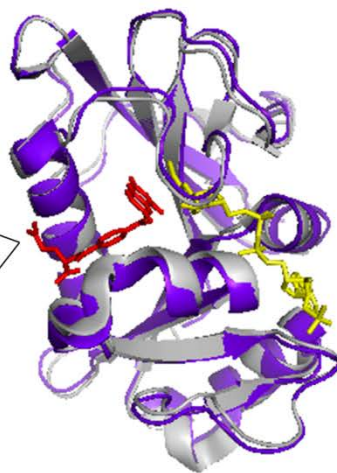


Figure 3.1. Sequence and structure alignment of mDHFR and hDHFR. (A) Sequence alignment of mDHFR and hDHFR. Phe31 is highlighted as bold and mismatching residues as red. (B) Structure alignment of mDHFR and hDHFR, shown is the enlarged view of the active site. Blue: mDHFR; Gray: hDHFR; Red: MTX bound to mDHFR; Purple: MTX bound to hDHFR. Phe31 and MTX are shown as sticks. (C) Structure alignment of mDHFR and hDHFR. Blue: mDHFR; Gray: hDHFR; Red: MTX; Yellow: NADPH. Figures are drawn with PyMOL.

3.2. Finding the target residue in the active site

In order to enhance the binding affinity of mDHFR toward its inhibitor (MTX) without compromising that of substrate DHF, several key residues for MTX and DHF binding in the mDHFR active site were identified first. The DHFR crystal structure [86] reveals that MTX directly contacts multiple residues including isoleucine7 (I7), leucine22 (L22), glutamic acid30 (E30), phenylalanine31 (F31), and asparagine64 (N64) in the active site of DHFR. These amino acids are highly conserved among mammalian DHFRs (Fig. 3.2), suggesting they are critical for the activity of DHFR. The mutations at those residues contacting MTX led to a decrease in the binding affinity while at the same time also resulted in varying degrees of loss in the substrate binding affinity. The high degree of structural similarity between DHF and MTX (Fig. 3.3) has made it challenging to selectively reduce the binding affinity to MTX without compromising the binding affinity to DHF.

Among the five key residues (I7, L22, E30, F31, and N64) that are critical for MTX binding, F31 was chosen in this study for SINA to alter the inhibition by MTX. Fig. 3.4 shows several key residues as well as their interactions with bound ligand as resolved in the crystal structure of hDHFR^{WT}:MTX and hDHFR^{WT}:FOL (files from PDB). F31 contribute to stabilize the MTX in the active site via π - π interaction, while it is not the case for FOL binding. This suggests the possibility of alleviating MTX binding while maintaining the affinity with substrate. Furthermore, more than forty phenylalanine analogs have been successfully incorporated into target proteins in a site-specific manner, and this offers a larger number of options to modify the active site of mDHFR more precisely, so as not to harm the binding of DHF [68,91].

	1	20	40	60	70
Mouse	MVRPLNCIVAVSQNMGIGKNG	DLPWPPLRNEFKYFQRM	TTT	SSVEGKQNLVIMGRKTWFSI	PEKNRPLKDI
Rat	MVRPLNCIVAVSQNMGIGKNG	DLPWPLLRENEFKYFQRM	TTT	SSVEGKQNLVIMGRKTWFSI	PEKNRPLKDI
Human	MVGSRLNCIVAVSQNMGIGKNG	DLPWPPLRNEFRYFQRM	TTT	SSVEGKQNLVIMGKKTWFSI	PEKNRPLKGI
Monkey	MVSSLNCIVAVSQNMGIGKNG	DLPWPPLRNEFRYFQRM	TTT	SSVEGKQNLVIMGKKTWFSI	PEKNRPLKGI
Cattle	MVRPLNCIVAVSQNMGIGKNG	NLPWPPLRNEFQYFQRM	TTV	SSVEGKQNLVIMGRKTWFSI	PEKNRPLKDI
	** .*****	:****:*****:*****.	*****:*****	*****.*	*****.*

Figure 3.2. Multiple sequence alignment of mammalian DHFRs. The amino acid sequences obtained from five different mammals (mouse, rat, human, monkey, and cattle) were aligned (: = conserved residues; = semi-conserved residues; * = strictly conserved residues).

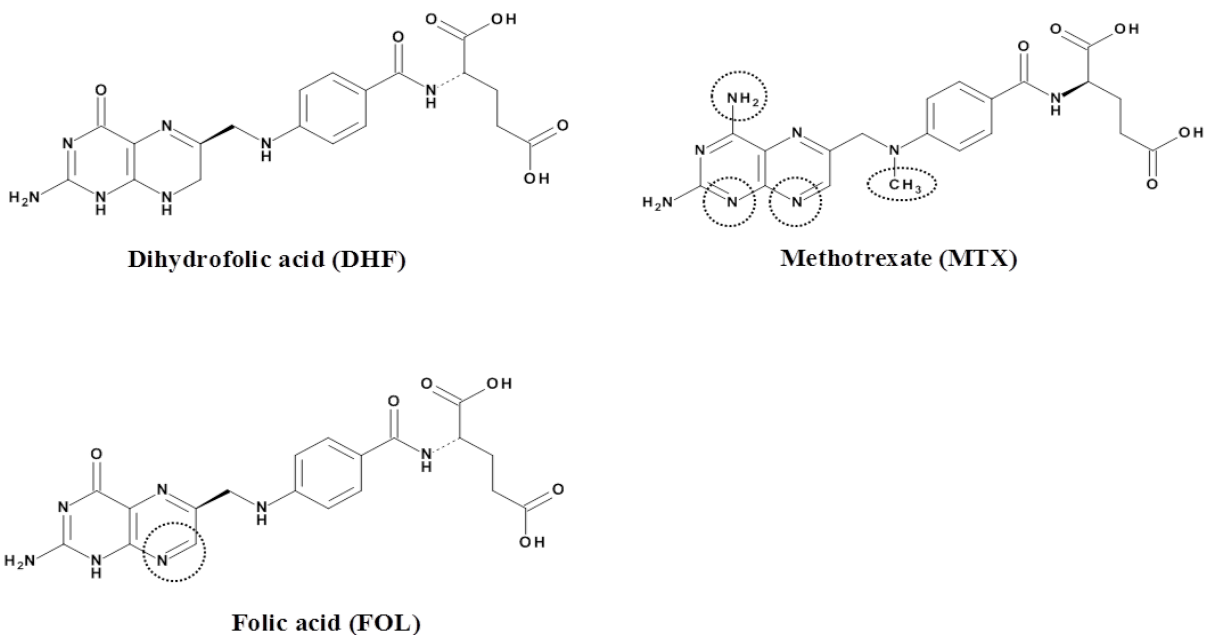


Figure 3.3. Chemical structure of substrate DHF and inhibitor MTX. MTX is a competitive inhibitor for mDHFR whose structure is similar to DHF.

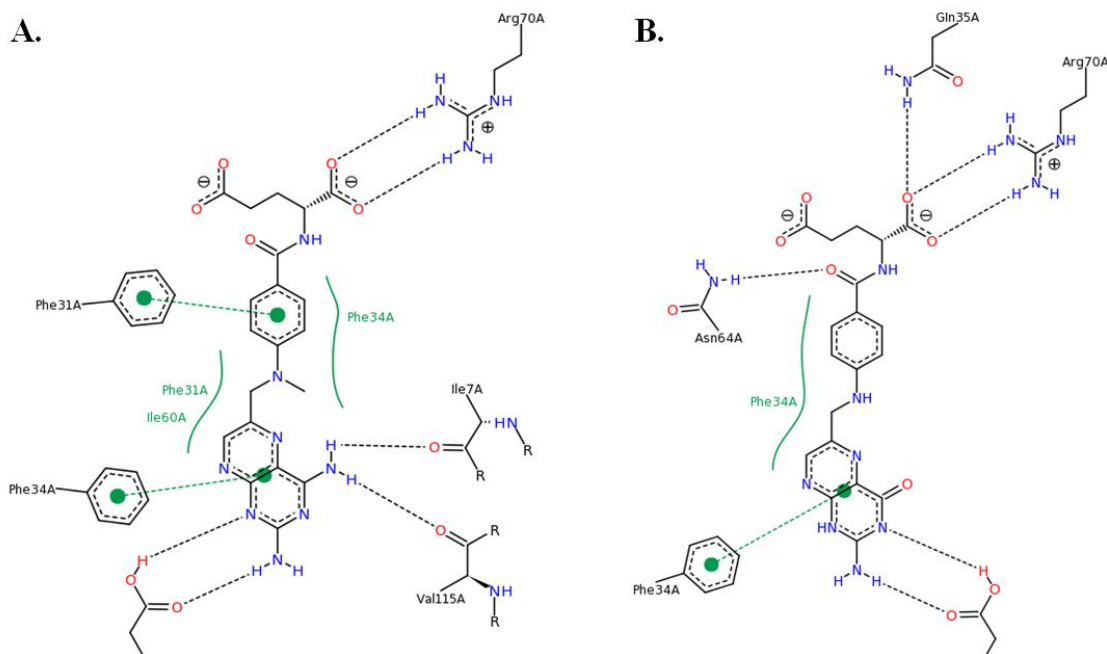


Figure 3.4. Interactions of key residues in the active site of hDHFR^{WT} with MTX or FOL (Figures from PDB). (A) hDHFR^{WT}:MTX; (B) hDHFR^{WT}:FOL. Black dashed line: hydrogen bonds, salt bridges, metal interactions; Green solid line: hydrophobic interactions; Green dashed line: π - π , π -cation interactions.

3.3. Non-natural amino acid mutagenesis *in silico*

Next, the NAAs to be used to mutate the position 31 were determined. In order to restrict MTX binding, Phe analogs pBrF and 2Nal which respectively has a side chain slightly and substantially bigger than Phe, were taken into consideration (Fig. 3.5). Then, structural models of the two variants bound with the inhibitor or substrate were constructed to predict the effects of replacement of F31 by pBrF or 2Nal on its inhibitor and substrate binding (Fig. 3.6).

In order to replace F31 with pBrF or 2Nal *in silico*, rotamer structural files of pBrF and 2Nal were obtained from the SwissSidechain database [94]. The PyMOL graphic software [95] was used to generate structure models containing pBrF or 2Nal at position 31 based on

hDHFR^{WT}:MTX (PDB ID: 1U70 and 2W3M). The rotamer of pBrF or 2Nal was chosen by maintaining favorable interactions while minimizing steric clash with the other hDHFR side chains. The crystal structures and the structural models are shown in Fig. 3.6. The inhibitor MTX directly contacts with the F31 phenyl ring (Fig. 3.6, top left panel). Therefore, replacing F31 with 2Nal containing a bulkier side chain leads to steric clash with the MTX (Fig. 3.6, top right panel), whereas replacing F31 with pBrF containing an additional bromine atom causes minimal steric clash with the MTX (Fig. 3.6, top middle panel). In contrast to the tight contact between the phenyl ring of F31 and MTX, there is bigger space between the F31 phenyl ring and its substrate (Fig. 3.6, bottom left panel). The space is big enough to accommodate the bulkier side chain of 2Nal in the active site without the steric clash with the substrate (Fig. 3.6, bottom right panel). As expected, pBrF at position 31 does not cause any noticeable clash with the substrate (Fig. 3.6, bottom middle panel). Therefore, from the structural models of mDHFR:ligand complexes, it is expected that replacing F31 with 2Nal will substantially restrict its inhibitor binding with a minimal substrate binding perturbation. Replacing F31 with pBrF will not affect its binding to both the inhibitor and the substrate.

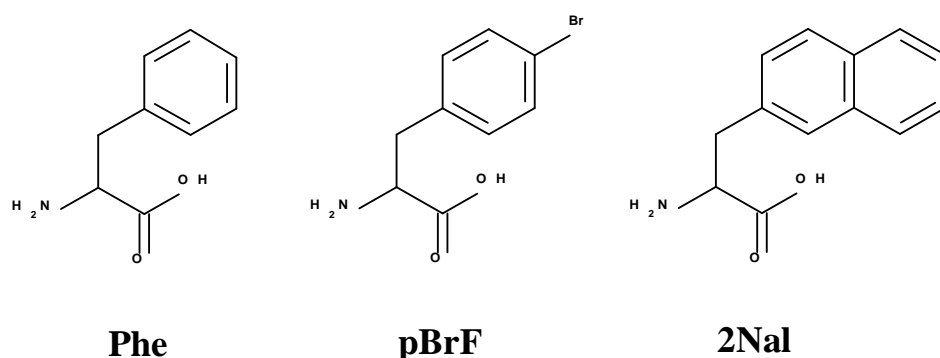


Figure 3.5. Chemical structure of phenylalanine (Phe), *p*-bromophenylalanine (pBrF), and *L*-2-naphthylalanine (2Nal).

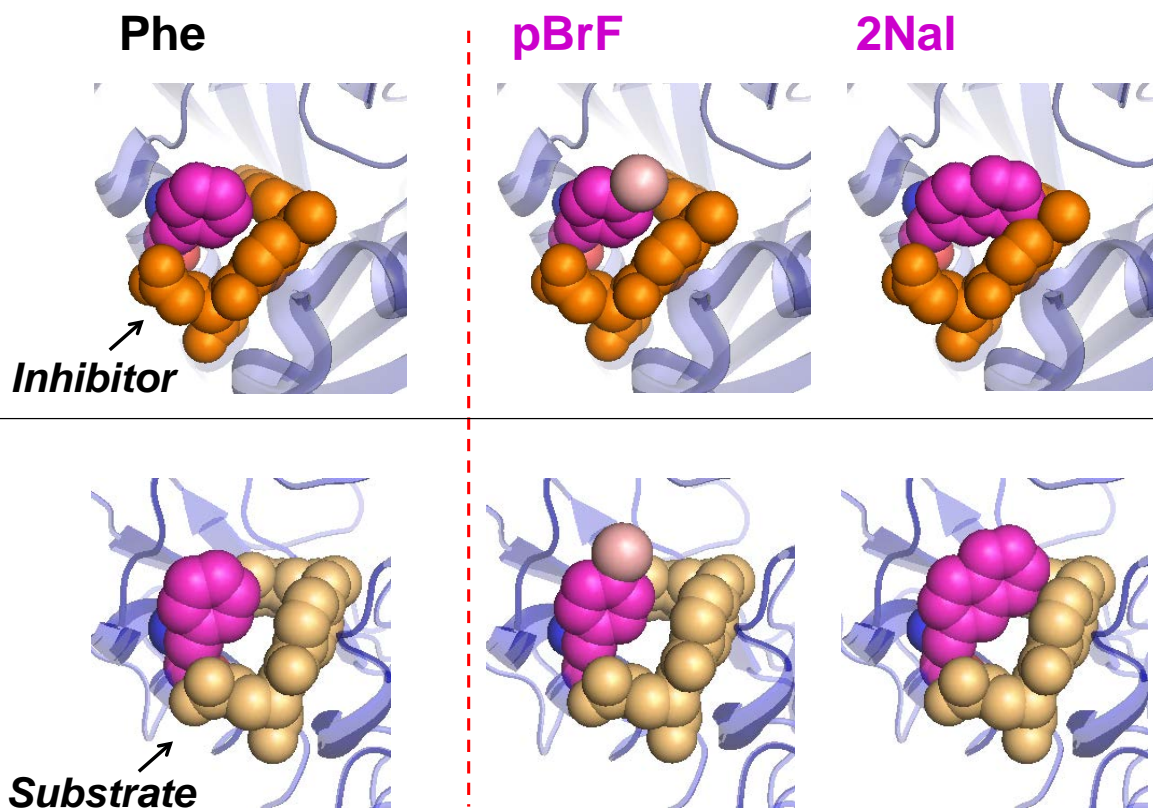


Figure 3.6. Structural models of mDHFR:ligand complexes. Variants with F31 are real crystal structures obtained from PDB, while variants with pBrF31 or 2Nal31 are constructed structural models. The crystal structure of hDHFR^{WT}:inhibitor (PDB ID: 1U72) (*top left*); the structural model of mDHFR^{pBrF31}:inhibitor (*top middle*) and mDHFR^{2Nal31}:inhibitor complex (*top right*). The structural models of mDHFR^{WT}:substrate (wild-type human DHFR:folate complex; PDB ID:2W3M) (*bottom left*); mDHFR^{pBrF31}:substrate (*bottom middle*) and mDHFR^{2Nal31}:substrate (*bottom right*). Inhibitor (orange); substrate (bright orange); carbon atom in side chain (magenta); bromine atom in side chain (light pink).

4. Preparation of Three mDHFR Samples

4.1. Theory

The schematic diagram for process of preparation of mDHFR variants (mDHFR^{WT}, mDHFR^{pBrF31}, and mDHFR^{2Nal31}) were shown in Fig. 4.1. mDHFR variants were separately expressed by *E. coli* cells, purified and the incorporation of pBrF and 2Nal were confirmed by matrix-assisted laser desorption-ionization time-of-flight mass spectroscopy (MALDI-TOF MS) of their tryptic digests.

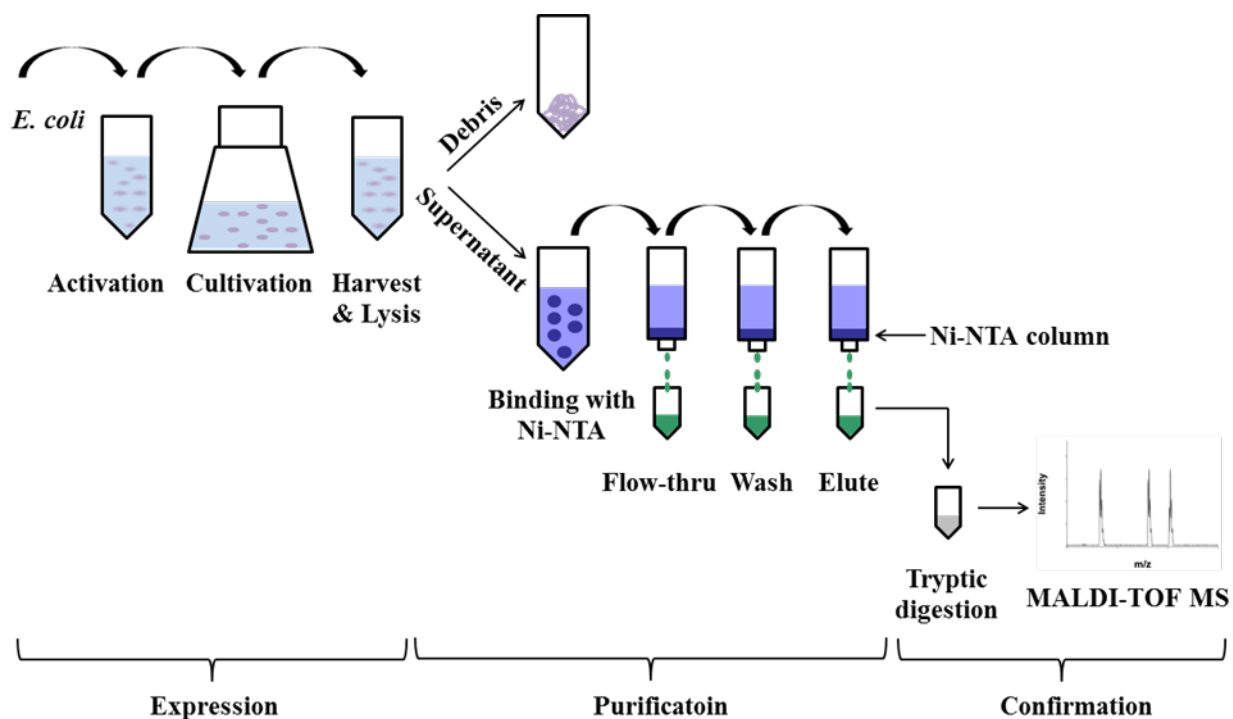


Figure 4.1. Schematic diagram for the preparation of mDHFR variants.

In this study, NAAs were incorporated into mDHFR by *E. coli* in a site-specific manner. To utilize the biosynthetic machinery of *E. coli* cells to incorporate NAA into target proteins, one

can add a separate set of elements for NAA, mimicking the way that the *E. coli* cells use to synthesize their native proteins with natural amino acids (Fig. 4.2). Protein synthesis inside the cell occurs at the ribosome, and the synthetic process is initiated by its binding with mRNA template

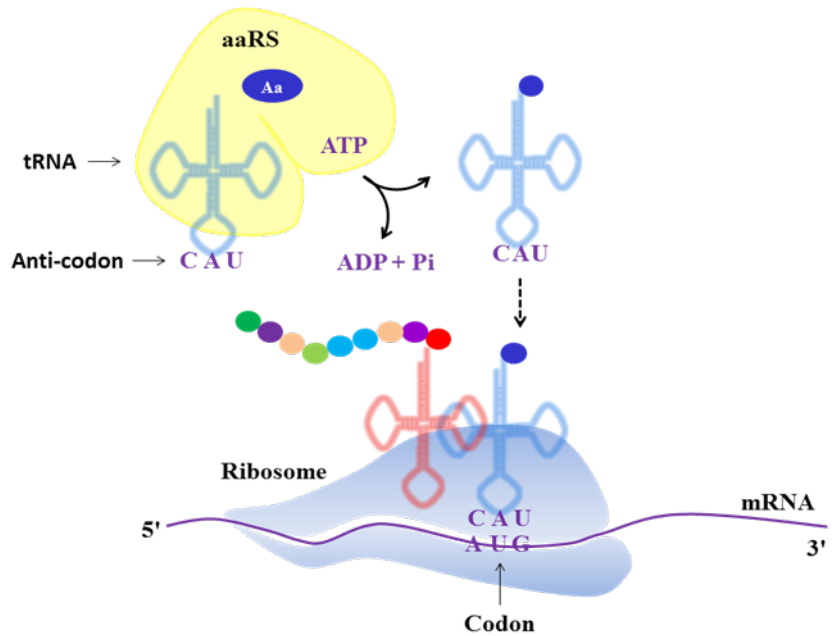


Figure 4.2. Translation process in *E. coli*.

which contains the information of amino acid sequence. Amino acids are delivered from the cytosol to the ribosome by a carrier called tRNA, the linkage of which is catalyzed by a highly specific enzyme aminoacyl-tRNA synthetase (aaRS). After charging with corresponding amino acid, tRNA moves to the ribosome and binds with mRNA based on codon and anti-codon base pairing, thus enabling the determination of amino acid sequence by that of messenger RNA (mRNA). Thus, an incorporation set consisting of a non-natural amino acid (NAA), a unique codon and aaRS/tRNA pair, which should not have any cross-talk with those inside the cell, should be designed, generated and imported into the cell. Each member of the set should meet a certain requirements to achieve a successful incorporation. First, the NAA must be readily uptaken, metabolically stable, non-toxic to the host cell *E. coli*, and also tolerated by the ribosome. Additionally, all NAAs should not be recognized by any endogenous aaRS, otherwise they will be incorporated to unexpected positions of both the target protein and native

proteins. In general most NAAs added to the media are taken up by the cells except for some highly charged ones which can be modified as metabolically labile derivatives or incorporated into dipeptides to increase permeability. Second, for the codon to be assigned to a NAA, a variety of alternatives have been developed, including non-natural base pair, four base codon as well as amber codon, among which amber codon is most popular. Amber codon a stop codon that doesn't encode any natural amino acid, instead is recognized by a release factor RF1 and terminates the protein synthesis. Among three stop codons (amber codon "UAG", ochre codon "UAA", and opal codon "UGA") used by *E. coli*, amber codon is chosen because it's the least used one by *E. coli* (relative usage of 9% compared with 62% and 30% for the latter two) so that potential harmful effects by reassigning to NAA can be minimized. Third, an orthogonal pair of aaRS/tRNA, which recognizes the NAA but at the same time doesn't cross-talk with the endogeneous components, should be imported. This criterion is thought to be the most challenging to fulfill. A most straightforward strategy is to choose the pair from a different kingdom and make modifications thereafter. For example, prokaryotic cell *E. coli* is to be used here as incorporation host, then the orthogonal pair is likely to be found in eukaryotic cells such as yeast. The Schultz group did an excellent work on this area by a two-step process involving both positive and negative rounds of selection to identify functional pairs without cross-talk [96]. Kwon et al. developed a good-quality system composed of an auxotrophic *E. coli* strain as well as a pair of aaRS/tRNA for *in vivo* incorporation of various NAAs into target mDHFR with high fidelity and yield, and this system was used in this study [68,91].

To facilitate the purification, six-histidine-tag (6xHis tag) was added to the C-terminus of mDHFR when constructing the plasmid. The attachment of several flanking residues at N-terminus as well as C-terminal including 6xHis tag was not expected to pose risk on inactivation

of mDHFR since they were far away from the active site, and this was further confirmed by the activity test performed later. Fig. 4.3 showed the active site of mDHFR where the inhibitor MTX and cofactor NADPH were bound, as well as the positions of N- and C- terminus. The figure also showed that C-terminus where 6xHis tag was located was at the surface of the molecule, rendering its affinity with nickel-nitrilotriacetic acid (Ni-NTA) resin at its native state.

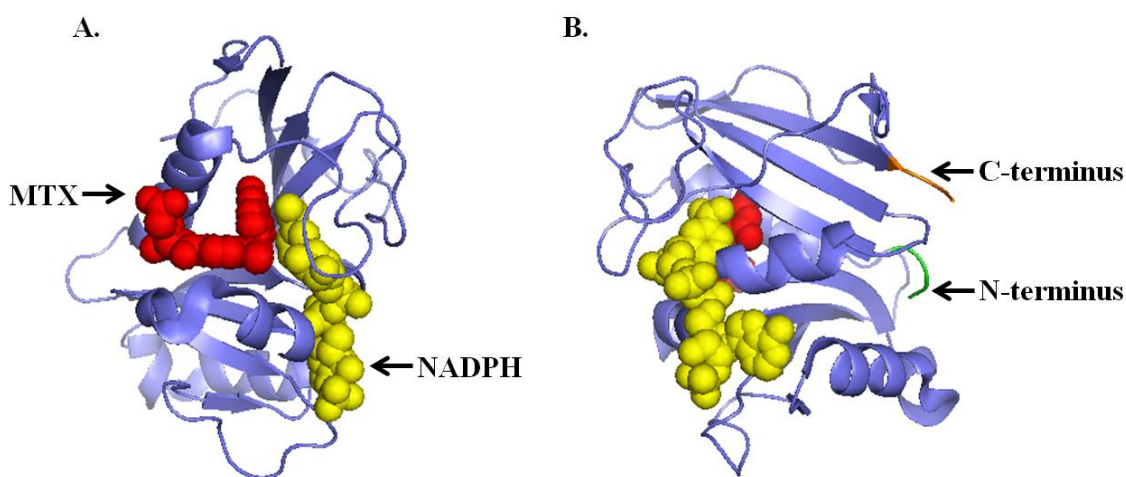


Figure 4.3. Crystal structure of mDHFR (PDB ID: 1U70) complexed with MTX (red) and NADPH (yellow). (A) Front view showing bound MTX and NADPH. (B) Side view, N-terminus was shown as green and C-terminus as orange.

6xHis-tag is one of the most widely used tags for purification of recombinant proteins that are expressed in the *E. coli* [97]. NTA immobilized on the resin, occupies four of six available binding sites in the coordination sphere of the nickel ion, remaining two sites for binding with 6xHis tag that is fused with target proteins (Fig. 4.4). After washing step in which nonspecifically bound contaminating proteins were removed, the target protein can be eluted with a high concentration of histidine analog imidazole. The initial trial of purification of

mDHFR^{WT} showed a certain level of impurities in the eluted sample thus a rough optimization of washing step was done by moderately increasing the imidazole concentration.

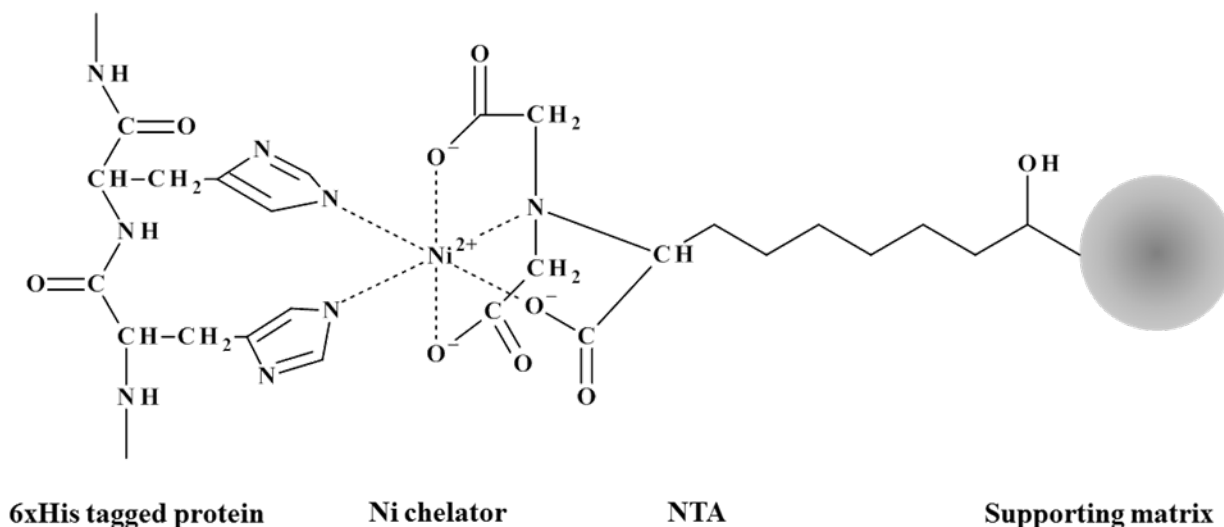


Figure 4.4. Binding of 6xHis tag with Ni-NTA matrix.

Sodium dodecyl sulfate polyacrylamide gel electrophoresis (SDS-PAGE) was used to test the expression of mDHFR mutants, to track the purification process and to determine the purity of the target proteins. SDS-PAGE is a technique for separating proteins based on their size [98]. SDS binds to the protein at approximate ratio of 1.4:1 (w/w) and breaks up the secondary, tertiary and quaternary structure of proteins to generate linear polymer chains coated with negatively charged SDS. The resulting molecules will be separated when they move through a porous media to the anode within an electric field, the rate of which is a function of the length or molecular weight. Concentration of polyacrylamide determines the resolution and 12% SDS-polyacrylamide gel was used in this study.

Following the purification step, the concentrations of purified mDHFR variants were determined by Lowry method by measuring its absorbance at 280 nm, of which was mainly due to the aromatic rings of tryptophan and tyrosine residues in the protein sequences.

To confirm the incorporation of pBrF or 2Nal at the designated position 31 of mDHFR, purified samples were digested with trypsin to yield smaller peptide fragments that can be analyzed by matrix MALDI-TOF MS. Trypsin is a serine protease that specifically cleaves at the carboxylic side of lysine and arginine residues. Sequencing grade modified trypsin in this study was modified by reductive methylation at its lysine residues to prevent autolytic digestion [99].

To prevent the inhibition of the ionization efficiency by salts, the digested mixture was then subjected to desalting according to the hydrophobic interaction of peptides with the alkane chains packed in a small tip.

MALDI-TOF MS has been used as a highly popular tool to analyze peptides and their modifications providing fast and extensive information on their composition. MALDI is a soft ionization technique particularly suitable for the analysis of biomolecules which otherwise will undergo significant decomposition. The resulting spectrum can be easily analyzed without complex data processing since single-charged, nonfragmented ions are predominantly generated in this technique. In MALDI-TOF MS, peptide samples are mixed with so-called matrix which is typically crystalline structured small organic compounds. Upon irradiation by the laser light, the matrix decomposes and transfers the energy to the peptides leading to their ionization. Subsequently, extracted and accelerated through the electric field, ions fly through in a vacuum to the detector during which they are separated by mass to charge ratio [100,101].

4.2. Materials and Methods

Twenty natural amino acids, antibiotics, isopropyl- β -D-thiogalactopyranoside (IPTG), *L*-(-)-fucose and 2,5-dihydroxybenzoic acid (DHB) were purchased from Sigma (St. Louis, MO). *p*-bromophenylalanine (pBrF) and *L*-2-naphthylalanine (2Nal) were obtained from Chem-Impex (Wood Dale, IL). The nickel-nitrilotriacetic acid affinity column (Ni-NTA column) and was purchased from Qiagen (Valencia, CA). Sequencing grade modified trypsin was procured from Promega (Madison, WI). ZipTip pipette tips containing C₁₈ reversed-phase media was obtained from Millipore (Billerica, MA). All other chemicals, unless otherwise noted, were purchased from Fisher Scientific (Pittsburg, PA) and were used without further purification. Cell growth media and all related solutions were either autoclaved at 121 °C for 20 min or filtered with 0.2 μ m filter for sterilization.

Lab Companion SI-600 Benchtop Shaker was from MIDSCI (St. Louis, MO). UV/VIS spectrophotometer Model DU-50 and centrifuge Model Avanti™ J-25 were from Beckman Coulter (Brea, CA). Ultrasonic dismembrator Model 500 was from Fisher Scientific (Pittsburg, PA). Large capacity sterilizer Model 3870M was from Tuttnauer (Hauppauge, NY). Nanodrop spectrophotometer 1000 was from Thermo Fisher Scientific (Wilmington, DE). SDS-PAGE image was taken by BioSpectrum imager from UVP (Upland, CA). Microflex™ MALDI-TOF MS was from Bruker (Billerica, MA).

mDHFR^{WT} was expressed using the *E. coli* XL1-Blue cells transformed with the plasmid pQE-16 which originally contains DNA sequence encoding wild-type mDHFR as well as β -lactamase. The cells were first cultivated in 3 mL of Luria–Broth (LB; 10 g/L tryptone, 5 g/L yeast extract, 10 g/L NaCl, pH 7.0) medium supplemented with 100 μ g/mL ampicillin, at 37 °C in a shaking incubator at 200 rpm. 1 mL of the seed culture was inoculated to 100 mL of LB medium supplemented with 100 μ g/mL ampicillin and cultivated at 37 °C at 200 rpm, until

OD₆₀₀ reached 0.6. Then IPTG was added to a final concentration of 1 mM, and the cells were further incubated at 37 °C for 5 hrs before harvest. Harvested cells were stored at -80 °C until purification.

For *in vivo* incorporation of pBrF or 2Nal, a Phe/Trp/Lys triple auxotrophic *E. coli* strain AFWK was co-transformed with pREP4-ytRNA^{Phe}_{CUA_UG} encoding an ytRNA^{Phe} amber suppressor gene and either pQE16-31AmDHFR-yPheRS^{T415A} or pQE16-31AmDHFR-yPheRS^{naph} to generate the expression cells AFWK (pQE16-31AmDHFR-yPheRS^{T415A}/pREP4-ytRNA^{Phe}_{CUA_UG}) or AFWK (pQE16-31AmDHFR-yPheRS^{naph}/pREP4-ytRNA^{Phe}_{CUA_UG}), which were used to express mDHFR mutants containing pBrF (mDHFR^{pBrF31}) or 2Nal (mDHFR^{2Nal31}) at position 31, respectively. The cells were first incubated in M9 minimal medium (12.8 g/L Na₂HPO₄·7H₂O, 3 g/L KH₂PO₄, 0.5 g/L NaCl, 1 g/L NH₄Cl, 4% glucose, 2 mM MgSO₄, 0.1 mM CaCl₂) supplemented with 20 amino acids (25 µg/mL), and antibiotics (35 µg/mL of kanamycin and 100 µg/mL of ampicillin) overnight at 37 °C in a shaking incubator at 200 rpm. The seed cultures were inoculated to the fresh minimal medium with the same composition as the seed culture and incubated at 37 °C at 200 rpm until OD₆₀₀ reached 0.8~1.0. Then cells were sedimented by centrifugation at 4,000 g for 10 min at 4 °C, washed twice with cold 0.9% NaCl, and shifted to the M9 medium supplemented with 17 amino acids (at 25 µg/mL), the rest three amino acids (Phe, Trp, and Lys), and 3 mM of either pBrF or 2Nal. 3 µM of Phe, Trp and Lys were used for the expression of mDHFR^{2Nal31}, while for mDHFR^{pBrF31}, the same concentration of Trp and Lys but 1 µM of Phe were used instead. After 10 min of incubation, protein expression was induced by addition of 1 mM IPTG, and the temperature was shifted to 30 °C. The cells were further incubated for 5 hrs before harvest. Harvested cells were stored at -80 °C until purification.

Purification of mDHFR^{WT}, mDHFR^{pBrF31}, and mDHFR^{2Nal31} was performed using Ni-NTA resin under the native condition with minor modification of the manufacturer's protocol (Qiagen). Cells were first thawed on ice for 15 min, suspended in the buffer and disrupted by sonication. Sonication was performed on an ice bath with amplitude of 10%, alternate 10s-on and 10s-off for a total time of 1 h. Cell debris and soluble part of the cell components were then separated by centrifugation at 10,000 g for 1 h at 4°C. The supernatant containing mDHFR^{WT} was mixed with Ni-NTA resin, and incubated in an ice bath with shaking at 200 rpm for 1 h. Subsequently, the resulting mixture was packed on a column, washed with washing buffer containing 40 mM of imidazole, and eluted several times with elution buffer containing 250 mM imidazole. The elution part with appropriate purity was chosen for further analysis.

Purity of purified mDHFR variants was determined by analyzing SDS-PAGE. The protein gel images were taken by UVP BioSpectrum imager and then analyzed by VisionWorks image analysis software. Protein concentration was determined by Beer's law with its absorbance at 280 nm, and a calculated extinction coefficient of 24,750 cm⁻¹ M⁻¹ [102].

Purified mDHFR variants were first subjected to trypsin digestion. Concentration of mDHFR variants were adjusted to 3 μM with elution buffer (50 mM NaH₂PO₄, 300 mM NaCl, and 10 mM imidazole), and 10 μL of each sample was diluted with freshly prepared 90 μL of 75 mM NH₄HCO₃. Tryptic digestion was performed with 1 μL of trypsin by incubating at 37°C for 2 hrs and the reaction was stopped by adding 12 μL of 5% trifluoroacetic acid (TFA) solution. The expected peptide fragments of the tryptic digests of mDHFR was generated via the online server ExPASy SIB Bioinformatics Resource Portal (<http://www.expasy.org/>). The peptide fragment “NGDLPWPPLRNE**FK**” (residues 18-32), containing the Phe residue at position 31 which was highlighted as bold, served as the reporter peptide (ref). According to the server, the

expected monoisotopic mass of the reporter peptide is 1682.86. Thus, replacement of Phe at position 31 by pBrF will lead to increase by about 80.18 Da while for 2Nal it will be 50.43 Da.

Peptide cleavage products were subjected to desalting on ZipTip pipette tips containing C₁₈ reversed-phase media according to the manufacturer's protocol (Millipore). 20 mg/mL of DHB and 2 mg/mL of *L*-(-)-fucose dissolved in 10% ethanol was used as the matrix for MALDI-TOF MS analysis.

4.3. Results and Discussion

4.3.1. Expression of mDHFR^{WT}, mDHFR^{pBrF31}, and mDHFR^{2Nal31}

Fig. 4.5 shows the SDS-PAGE data for the protein profiles before and after induction for the three mDHFR variants.

The size of mDHFR^{WT} used in this is around 23.3 kDa as calculated by the online server PeptideMass (Swiss Institute of Bioinformatics, http://web.expasy.org/peptide_mass/). Comparing the protein profile of cells for the expression of mDHFR^{WT} before and after induction (Fig. 4.5, Lane 2 and 3), a clear thick band appeared between 22 and 31 kDa. It was not surprising to see a much lower expression level of mDHFR mutants (Fig. 4.5, Lane 5 and 7) than mDHFR^{WT} (Fig. 4.5, Lane 3). For generation of mDHFR mutants with higher fidelity, M9 minimal media were used instead of LB complex media which could supply more nutritious environment for faster cell growth as well as protein expression. Additionally, the concentration of three essential natural amino acids (Phe, Trp and Lys) were limited to a certain low level considering their misincorporation into the targeted position 31 of mDHFR mutants [68,91]. Furthermore, possible recognition of pBrF or 2Nal by native *E. coli* aaRSs leading to their incorporation into native *E. coli* proteins, though not detrimental as the cells successfully grew here, may also contribute. Since the clarification of the mechanism was not within the scope of

this study, and mDHFR variants were obtained to a certain level, purification was performed with these cells directly.

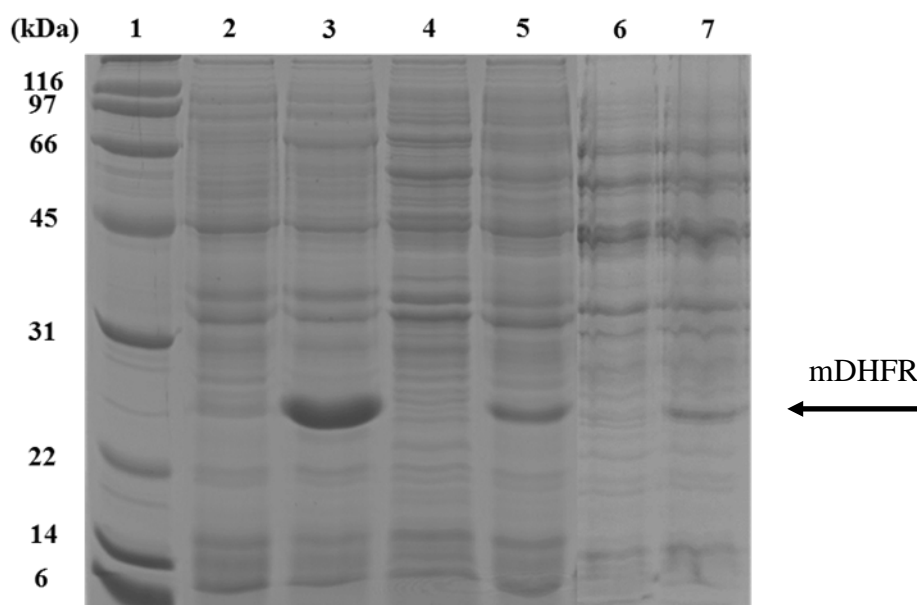


Figure 4.5. SDS-PAGE data for confirmation of the expression of mDHFR^{WT}, mDHFR^{pBrF31}, and mDHFR^{2Nal31}. Lane 1: marker, the size of each band is shown on the left; Lane 2: cells for mDHFR^{WT} expression, before induction; Lane 3: cells expressing mDHFR^{WT}, after induction; Lane 4: cells for mDHFR^{pBrF31} expression, before induction; Lane 5: cells expressing mDHFR^{pBrF31}, after induction; Lane 6: cells for mDHFR^{2Nal31} expression, before induction; Lane 7: cells expressing mDHFR^{2Nal31}, after induction.

4.3.2. Purification of mDHFR^{WT}, mDHFR^{pBrF31}, and mDHFR^{2Nal31}

For comparison of the binding affinity of mDHFR variants, it's essential to purify them at their active forms. The next step was to determine which compartment of cells the mDHFR variants were expressed. Preferably, their expression as soluble forms in the cell cytosol would greatly facilitate the following purification procedure, since it will help avoid the renaturing process after purification under denatured condition, which generally led to recovery of a small fraction of active proteins. The soluble and insoluble portions of sonicated cells were separated by centrifugation and SDS-PAGE was used to analyze the protein components in each of them.

As shown in Fig. 4.6, mDHFR^{WT} existed both in the soluble and insoluble (Fig. 4.6.A, Lane 2 and 3) portions of the cells after treatment with sonication, while the majority of mDHFR^{pBrF31} went to the soluble portion (Fig. 4.6.B, Lane 2). The solution appeared much less viscous and translucent compared before disruption, suggesting cells should have been ruptured almost completely. The existence of the target band mDHFR^{WT} in the insoluble fraction might be due to the high-level expression of mDHFR^{WT} under the current expression condition, as they tend to form insoluble aggregates called inclusion body at high concentration inside the cell. The formation of inclusion body for proteins expressed at high level has been observed consistently by many other studies [103,104]. This was further suggested by the result that mDHFR^{pBrF31} was expressed mostly as soluble form, who was expressed relatively moderately as shown in Fig. 4.6. Local heat effect near the probe of the sonicator during sonication process, despite ice bath was used to relieve this phenomenon, may also helped the aggregation of a small amount of proteins. For mutant mDHFR^{2NaI31}, it was the same case as mDHFR^{pBrF31}. The soluble fractions prepared as above were undergone purification with Ni-NTA column and the procedure was tracked by the analysis with SDS-PAGE.

Fig. 4.7 showed the purified mDHFR^{WT}, mDHFR^{pBrF31}, and mDHFR^{2NaI31}, with purity of 87.0%, 95.8%, and 96.0%, respectively.

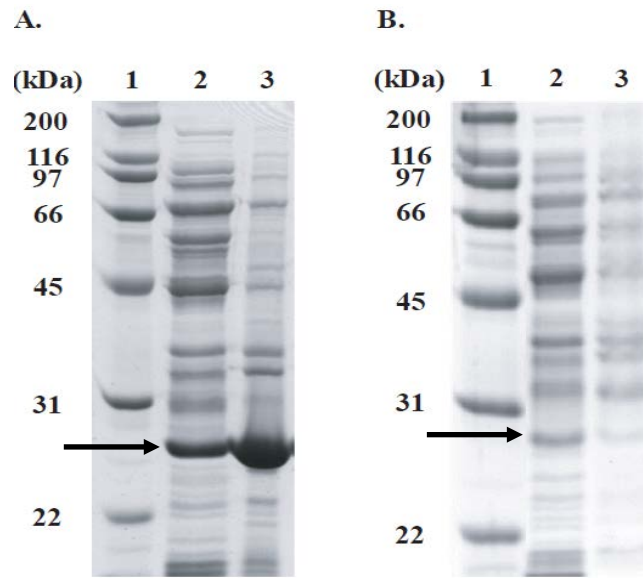


Figure 4.6. SDS-PAGE data for soluble and insoluble portion of cells expressing mDHFR^{WT} and mDHFR^{pBrF31}. (A) mDHFR^{WT}. Lane 1: marker, the size of each band was shown on the left; Lane 2: soluble portion; Lane 3: insoluble portion. (B) mDHFR^{pBrF31}. Lane 1: marker, the size of each band was shown on the left; Lane 2: soluble portion; Lane 3: insoluble portion. mDHFR variants were indicated with arrow.

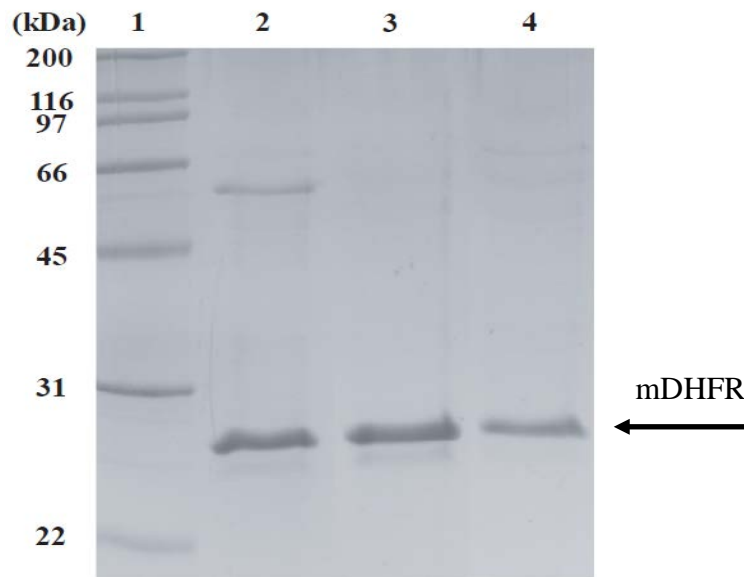


Figure 4.7. SDS-PAGE of purified mDHFR variants. Lane 1: maker, the size of each band was shown on the left; Lane 2: mDHFR^{WT} (87.0% purity); Lane 3: mDHFR^{pBrF31} (95.8% purity); Lane 4: mDHFR^{2NaI31} (96.0% purity).

4.3.3. MALDI-TOF MS for Confirmation of pBrF and 2Nal Incorporation

Tryptic digests of mDHFR variants were analyzed to determine the occupancy of the amber codon, after which the resulting peptide fragments could be readily analyzed by MALDI-TOF MS. A peptide consisting of residues from 18 to 32 (NGDLPWPPLRNEA*K, position 31 shown as *) served as the reporter peptide. In the mDHFR^{WT}, it was named Peptide_F31 (NGDLPWPPLRNEAFK). Peptide_F31 was detected with a monoisotopic mass of 1682.47 Da (Fig. 4.8), in accord with its theoretical mass (1682.86 m/z). In an mDHFR variant containing an amber codon, Peptide_Z31 (NGDLPWPPLRNEA Am K) contains the amber site (Am) at position 31. Peptide_Z31s containing pBrF and 2Nal at the amber site were denoted as Peptide_pBrF31 (NGDLPWPPLRNE pBrF K) and Peptide_2Nal31 (NGDLPWPPLRNE 2Nal K), respectively. In the presence of pBrF or 2Nal in the culture media, a strong signal at a mass of 1762.65 or 1732.90 Da was detected, respectively. Considering that the substitution of pBrF or 2Nal for Phe leads to a mass increase of 78.90 or 50.06 Da, the observed shift in the experimental mass by 80.18 or 50.43 Da was consistent with replacement of Phe by pBrF or 2Nal at the amber codon site, respectively, suggesting the successful incorporation at the designated position. Furthermore, the peak for mDHFR^{WT} was almost invisible in the spectra of two digested mDHFR mutants, suggesting high fidelity of the incorporation system used in this study. This guaranteed a fair comparison of the affinities of mDHFR variants with either inhibitor MTX or substrate DHF in the following chapter.

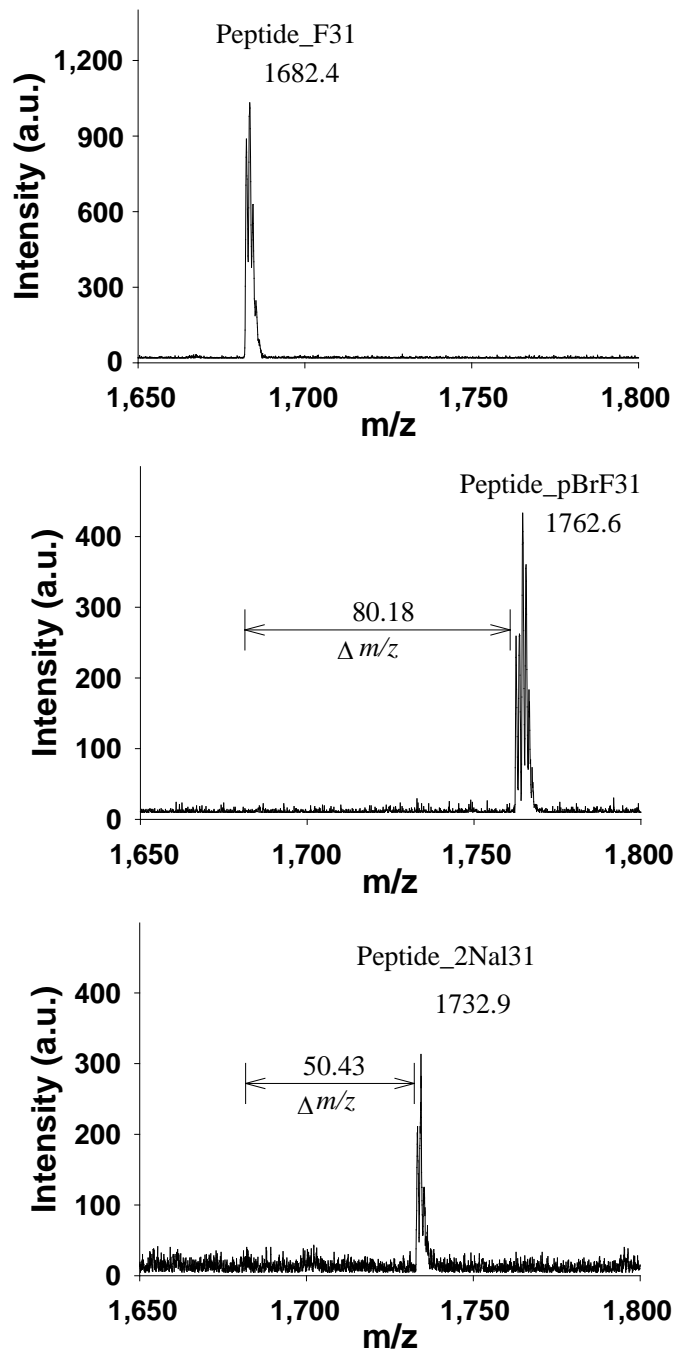


Figure 4.8. Incorporation of pBrF and 2NaI at mDHFR position 31 confirmed by MALDI-TOF MS of tryptic digests of mDHFR variants. Peptide_F31 refers to a tryptic fragment of mDHFR^{WT} (residues 18-32; NGDLPWPPLRNEAFK). Peptide_pBrF31 and Peptide_2NaI31 refer to the form of the peptides containing pBrF and 2NaI in place of Phe at position 31, respectively. See text for details.

5. Controlling Enzyme Inhibition with Non-natural Amino Acids

5.1. Theory

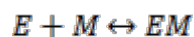
Table 5.1. Symbols and their physical meanings

Symbol	Physical meaning	Symbol	Physical meaning
K_D	Dissociation constant	K_M	Michaelis constant
$[E]_0$	Initial conc. of enzyme	k_{cat}	Turnover rate
$[E]$	Conc. of free enzyme	$[S]$	Conc. of free DHF
$[M]_0$	Initial conc. of MTX	$[ES]$	Conc. of enzyme-DHF complex
$[M]$	Conc. of free MTX	$[P]$	Conc. of THF
$[EM]$	Conc. of enzyme-MTX complex	Q	Quenched fraction of enzyme

5.1.1. Determination of Dissociation Constant

Trp, Tyr, and Phe can offer proteins with intrinsic fluorescence due to their aromatic structures. The possible occurrence of energy transfer among them, as well as stronger fluorescence compared with the other two, make Trp contribute most to the fluorescence of a protein. The fluorescence of the indole chromophore in Trp is highly sensitive to the environment, making it ideal to report the folding status of the protein. Binding of MTX to mDHFR can lead to the structural change of the latter thus a change in its intrinsic fluorescence. The quenching of Trp fluorescence of mDHFR upon binding of MTX has been used to measure the dissociation constant [92,105].

The binding of the enzyme mDHFR with inhibitor MTX can be expressed as the follows:



Where E is enzyme (in this case mDHFR), M is MTX and EM is enzyme-MTX complex.

Since

$$K_D = \frac{[E] \times [M]}{[EM]}$$

$$[E] = [E]_0 - [EM]$$

$$[M] = [M]_0 - [EM]$$

So,

$$K_D = \frac{([E]_0 - [EM]) \times ([M]_0 - [EM])}{[EM]}$$

$$\text{Since } Q = \frac{[EM]}{[E]_0}$$

So,

$$[EM] = [E]_0 \times Q$$

So,

$$K_D = \frac{1-Q}{Q} \times ([M]_0 - Q \times [E]_0)$$

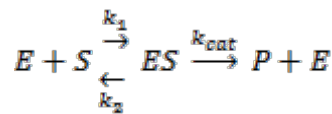
Solving for Q, we can get:

$$Q = \frac{([E]_0 + [M]_0 + K_D) - \sqrt{([E]_0 + [M]_0 + K_D)^2 - 4 \times [E]_0 \times [M]_0}}{2 \times [E]_0} \quad \text{(Equation 5.1.)}$$

With all other values known, the dissociation constant could be obtained by fitting a curve monitoring change of Q as a function of $[M]_0$.

5.1.2. Determination of Michaelis Constant

Kinetic parameters could be obtained using Michaelis-Menten model [106]. Michaelis constant K_M signifies the affinity between an enzyme and the substrate, and the smaller the K_M , the higher the affinity between the enzyme and substrate. The reaction scheme was as below:



Where E is enzyme (in this case mDHFR), S is substrate DHF, ES is enzyme-DHF complex and P is product THF.

With steady state assumption:

$$\frac{d[ES]}{dt} = k_1[E][S] - k_2[ES] - k_{cat}[ES] = 0$$

$$\text{Since } [E]_0 = [E] + [ES] \text{ and } r = \frac{d[P]}{dt} = k_{cat}[ES]$$

Where r is the substrate consumption rate, with unit of $\mu\text{M}/\text{sec}$.

Combining the above three, the rate can be expressed as:

$$r = \frac{k_{cat}[E]_0[S]}{K_M + [S]} \quad \text{(Equation 5.2.)}$$

$$\text{Where } K_M = \frac{k_2 + k_{cat}}{k_1}$$

So, fixing the concentration of the corresponding mDHFR variant, K_M and k_{cat} could be obtained by fitting a curve monitoring the change of reaction rate as a function of substrate DHF concentration.

5.2. Materials and Methods

Dihydrofolate reductase assay kit, methotrexate (MTX), dihydrofolic acid (DHF), and nicotinamide adenine dinucleotide phosphate (NADPH) were purchased from Sigma (St. Louis, MO). All other chemicals, unless otherwise noted, were purchased from Fisher Scientific (Pittsburg, PA) and were used without further purification.

Fluorolog-3 FL3-22 spectrofluorometer was from Horiba (Ann Arbor, MI). Synergy™ 4 multi-mode microplate reader was from BioTek (Winooski, VT).

The linear relationship between Trp fluorescence and enzyme concentration was checked with 25 ~ 2000 nM of mDHFR^{WT}.

Equilibrium dissociation constants between MTX and mDHFR variants were determined by measuring the quenching of Trp fluorescence when MTX bound to mDHFR, as described previously with minor changes [92]. Trp fluorescence was measured by excitation at 290 nm and emission at 350 nm. Various concentrations of MTX (0 to 1 mM) were added into the mDHFR solution, and the mixture was incubated for 10 min at room temperature before measuring tryptophan fluorescence. All the measurements were made in at least triplicate for each experimental condition. A fraction of mDHFR samples quenched (Q) was calculated from the fluorescence values. The data were fitted into a curve to determine K_D values using the Eqn. 5.1.

Kinetic assay of mDHFR was performed by measuring the change in absorbance at 340 nm caused by the consumption of cofactor NADPH in reference to the manufacturer's protocol (Sigma). Briefly, 60 μ M of NADPH and varying concentrations of DHF (1 to 50 μ M) were dissolved in 25 °C MTEN buffer (50 mM 2-(*N*-morpholino)ethanesulfonic acid, 25 mM tris(hydroxymethyl)aminomethane, 25 mM ethanolamine, and 100 mM sodium chloride, pH 7.5) and the reaction was initiated by the addition of enzyme to a final concentration of 22.8 nM. The absorbance was measured as soon as the enzyme was added in the reaction system. All the measurements were made in at least triplicate for each experimental condition.

5.3 Results and Discussion

5.3.1. Binding Affinity with Inhibitor MTX

In order to compare the binding affinities of mDHFR^{WT}, mDHFR^{pBrF31}, and mDHFR^{2Nal31} toward MTX, the Trp fluorescence quenching of mDHFRs over a broad range of MTX concentrations was monitored using a fluorimeter as previously reported [92]. As expected, the decrease of fluorescence quenching by MTX was in the order of mDHFR^{WT}, mDHFR^{pBrF31}, and mDHFR^{2Nal31} (Fig. 5.2). In the presence of 10 mM of MTX, the Trp fluorescence intensities of

mDHFR^{WT} and mDHFR^{pBrF31} were only 56% and 74% of that of mDHFR^{2Nal31} (Fig. 5.2). With the Trp fluorescence intensities of the mDHFR variants at varying concentrations of MTX, Q values (the percentages of mDHFR quenched) were calculated. Then, Q value vs. MTX concentration was plotted (Fig. 5.3). These data were fitted with Eqn 5.1 as described in the Theory section, in order to calculate the MTX dissociation constant (K_D) of different mDHFR variants. The calculated K_D values and the relative K_D values compared to that of mDHFR^{WT} (K_D (rel)) were shown in Table 5.2. K_D (rel) values for pBrF and 2Nal were 2.1 ± 1.1 and 4.3 ± 2.0 , respectively. K_D and K_D (rel) values were inversely correlated to the binding affinity of mDHFR toward MTX. Therefore, these results indicated that the binding affinities of mDHFR^{pBrF31} and mDHFR^{2Nal31} toward MTX were weaker than that of mDHFR^{WT} by about a factor of 2 and 4 times, respectively. As shown in the models of 3D mDHFR structures, replacing F31 with 2Nal containing a bulky side aromatic side chain (mDHFR^{2Nal31}) significantly reduced the binding affinity to MTX; most likely due to steric clash with MTX in the active site (Fig. 3.6; top right panel). Although replacing F31 with pBrF containing a slightly bulkier side chain than Phe also reduced the binding affinity to MTX, the extent was smaller compared to that of F31 with 2Nal.

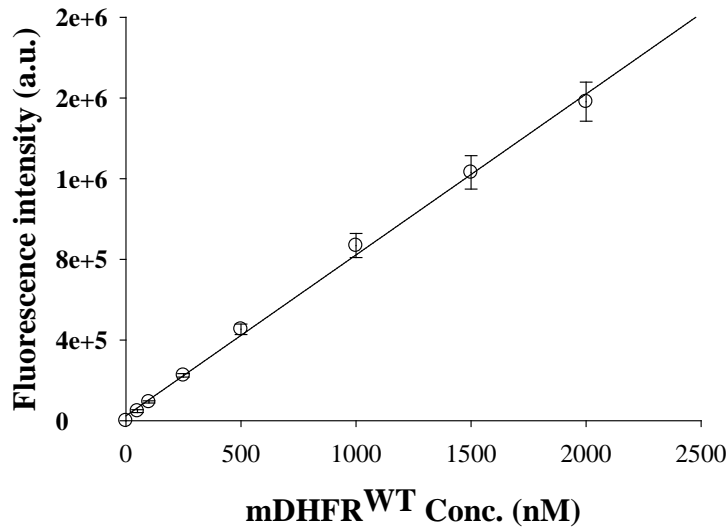


Figure 5.1. Linear relationship between tryptophan fluorescence and mDHFR^{WT} concentration. ($R^2=0.9978$; $n=3$).

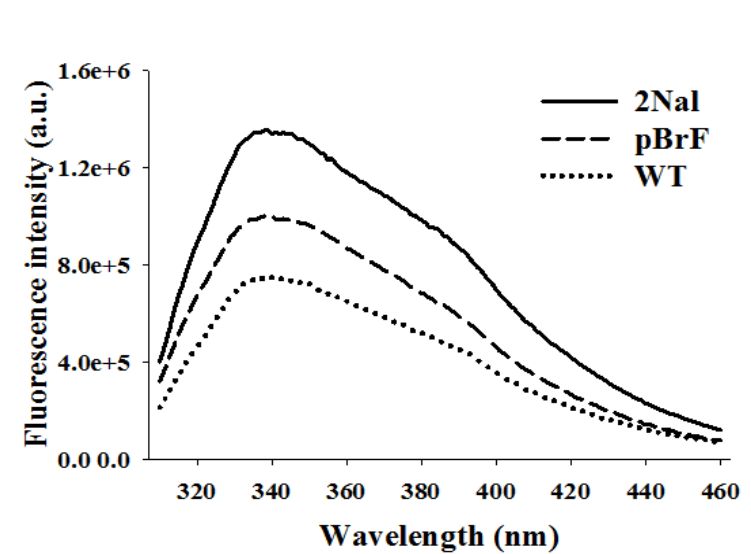


Figure 5.2. Tryptophan fluorescence spectra of the mDHFR samples in the presence of MTX. The tryptophan fluorescence of three mDHFR variants (WT: mDHFR^{WT}; pBrF: mDHFR^{pBrF31}; 2Nal: mDHFR^{2Nal31}) were quenched in the presence of 1.0×10^4 nM of MTX.

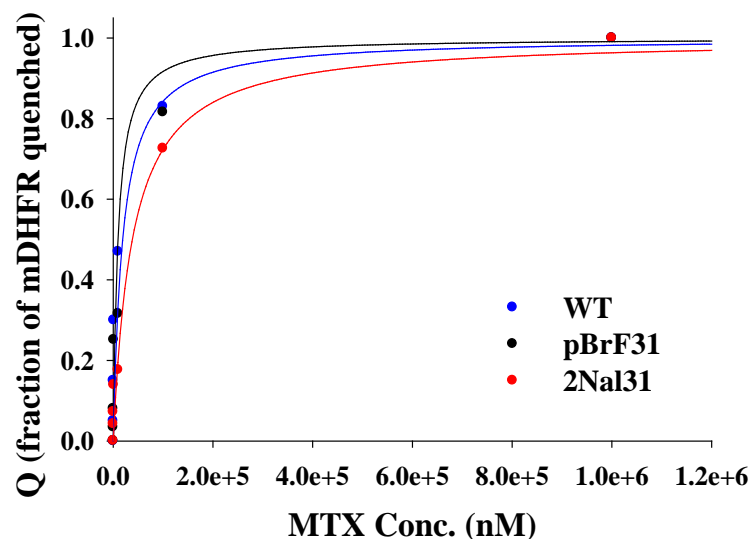


Figure 5.3. The fraction of mDHFR variants quenched (Q) at varying concentrations of MTX. WT: mDHFR^{WT}; pBrF31: mDHFR^{pBrF31}; 2Nal31: mDHFR^{2Nal31}. MTX concentration ranged from 0 to 1.0×10^6 nM. The data were fitted into a curve to determine K_D values using Eqn. 4.1.

5.3.2. Binding Affinity with Substrate DHF

Direct measurement of the binding affinity between a substrate and an enzyme is not trivial due to continuous conversion of substrate into product. Alternatively, Michaelis constant K_M , which is inversely correlated to substrate binding affinity, was obtained. In order to investigate the effects of the replacement of F31 with pBrF or 2Nal on the binding affinity of mDHFR toward its substrate DHF, reaction rates of the three mDHFR variants (mDHFR^{WT}, mDHFR^{pBrF31}, and mDHFR^{2Nal31}) were measured using a DHFR assay kit. The range of DHF concentration reaction rates were fitted into Michaelis-Menten model to calculate the kinetic parameters K_M and k_{cat} (Fig. 5.5, Table 5.2).

Fig. 5.4 showed a typical comparison of the activities of mDHFR^{WT}, mDHFR^{pBrF31}, and mDHFR^{2Nal31}, at 30 μ M of DHF and 60 μ M of NADPH. Among those three, mDHFR^{pBrF31} had

the highest activity while mDHFR^{2Nal31} the lowest one as suggested by the slowest DHF consumption rate. An approximate linear range could be observed during the initial 1-2 min of reaction, indicating the validity of the steady state assumption. As time proceeded, substrate was consumed continuously and the reaction rate slowed down continuously. The slopes within the initial stages were calculated to obtain the reaction rate of each variant under various DHF concentrations.

The K_M value of mDHFR^{WT} was 6.5 μM . The K_M values of mDHFR^{pBr31} and mDHFR^{2Nal31} were comparable to or slightly smaller than that of mDHFR^{WT} suggesting that the bulkier side chains of pBrF and 2Nal, as compared to Phe, might have more favorable contacts to the substrate DHF by filling up the space. The binding selectivity of mDHFR variants toward DHF over MTX is correlated to the ratio of K_D over K_M (K_D/K_M). The K_D/K_M values of mDHFR^{pBrF31} and mDHFR^{2Nal31} relative to that of mDHFR^{WT} were 3.9 and 5.6, respectively, indicating that replacing F31 with pBrF or 2Nal could selectively reduce the binding affinity toward the inhibitor MTX without compromising the binding to the substrate DHF. These findings were consistent with the predictions based on the structural models of DHFR variant-ligand complexes (Fig. 3.6). Despite the enhanced selectivity, it should be noted that replacing F31 with 2Nal led to an approximate 3-fold reduction in the catalytic efficiency (k_{cat}/K_M). We speculate that the bulky 2Nal side chain perturbed the active site structure, which consequently inhibited the electron flow of the catalytic reaction and thus reduced the catalytic efficiency. However, replacing F31 with pBrF moderately reduced the inhibitor binding affinity without compromising catalytic efficiency.

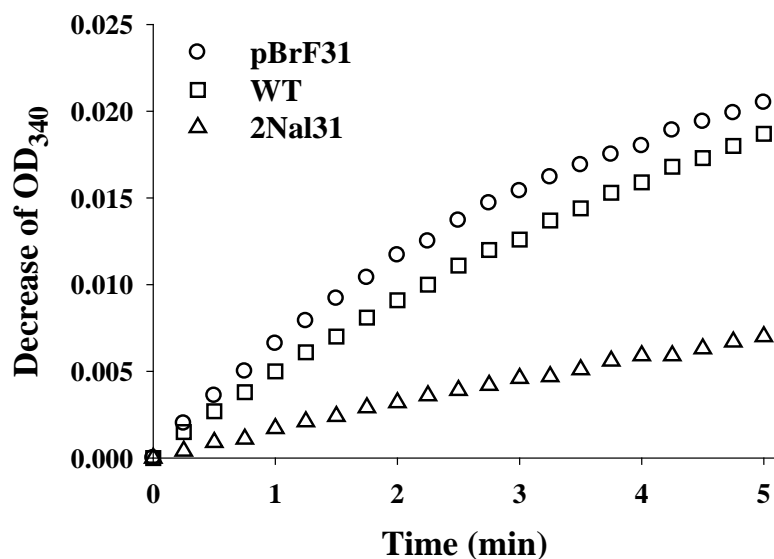


Figure 5.4. Comparison of reaction rate for three mDHFR variants. WT: mDHFR^{WT}; pBrF: mDHFR^{pBrF31}; 2Nal: mDHFR^{2Nal31}. Reaction was performed with 30 μM of DHF and 60 μM of NADPH dissolved in MTEN buffer.

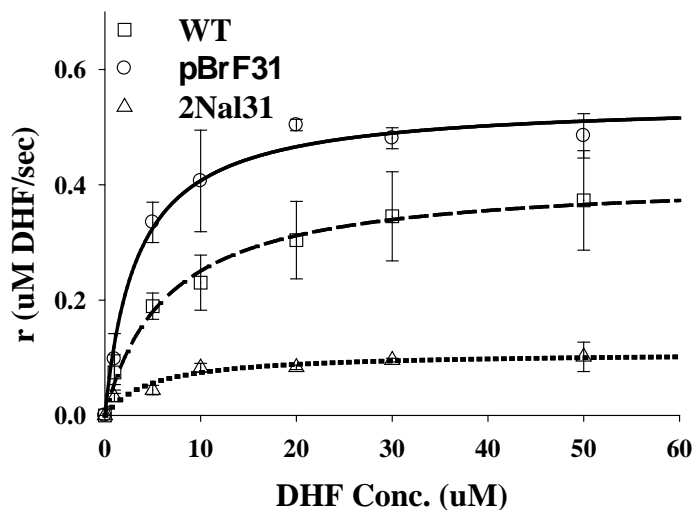


Figure 5.5. Enzyme reaction rate (μM of DHF consumed by per μM of enzyme per minute) at various concentrations of DHF. WT: mDHFR^{WT}; pBrF31: mDHFR^{pBrF31}; 2Nal31: mDHFR^{2Nal31}. DHF concentration ranged from 1 to 50 μM , $n=3\sim 5$. The data were fitted into a curve to determine K_M and k_{cat} values using Eqn. 4.2.

Table 5.2. MTX dissociation constants and kinetic parameters of mDHFR variants.

Variants	mDHFR^{WT}	mDHFR^{pBrF31}	mDHFR^{2NaL31}
K_D (μM)	8.9 \pm 3.8	18.4 \pm 6.4	37.9 \pm 8.8
K_D (rel) ^a	1.0 \pm 0.6	2.1 \pm 1.1	4.3 \pm 2.0
K_M (μM)	6.5 \pm 1.0	3.4 \pm 0.6	4.8 \pm 1.6
k_{cat} (sec^{-1})	0.32 \pm 0.01	0.42 \pm 0.02	0.084 \pm 0.007
K_D/K_M	1.4 \pm 0.6	5.4 \pm 1.7	7.9 \pm 2.1

^aRelative to K_D for mDHFR^{WT}

6. Conclusions

In this study, mDHFR as a model was engineered via site-specific incorporation of NAAs to reduce the inhibitor binding without compromising substrate binding.

1. The key residue (F31) to replace with NAAs was selected by analyzing homologous crystal structures of hDHFR. Structural models of mDHFRs containing the NAAs further suggested that the NAAs introduced into the active site restricts the inhibitor binding due to the steric hindrance.
2. Two NAAs, pBrF and 2Nal were successfully incorporated in the position 31 of mDHFR in site-specific way *in vivo*, as confirmed by the mass spectrometry.
3. Three mDHFR variants were successfully purified in a native form with a high purity.
4. The binding affinities of the purified mDHFR variants with inhibitor MTX and substrate DHF were measured and compared. Replacing F31 with 2Nal or pBrF containing a bulkier side chain reduced the inhibitor binding affinity by a factor of 2.1 ± 1.1 and 4.3 ± 2.0 , respectively. It also enhanced the selectivity toward the substrate DHF over the inhibitor MTX by a factor of 3.9 and 5.6, respectively. The catalytic efficiency of the mDHFR variant containing pBrF was comparable to that of the wild-type mDHFR, whereas the mDHFR variant containing 2Nal exhibited 2.8-fold lower catalytic efficiency. Uncertainties in the table were obtained during the regression progress and caution is required to interpret the results. Considering the error associated with single measurement, replicates of experiments are expected to reduce the uncertainty values.

This study demonstrated that enzyme inhibition can be precisely controlled by structure-based rational design combined with site-specific incorporation of the NAA.

References

1. Bornscheuer UT, Huisman GW, Kazlauskas RJ, Lutz S, Moore JC, Robins K: **Engineering the third wave of biocatalysis.** *Nature* 2012, **485**:185–94.
2. Arnold FH: **Combinatorial and computational challenges for biocatalyst design.** *Nature* 2001, **409**:253–7.
3. Schmid a, Dordick JS, Hauer B, Kiener A, Wubbolts M, Witholt B: **Industrial biocatalysis today and tomorrow.** *Nature* 2001, **409**:258–68.
4. Schoemaker HE, Mink D, Wubbolts MG: **Dispelling the myths--biocatalysis in industrial synthesis.** *Science* 2003, **299**:1694–7.
5. Jensen VJ, Rugh S: **Industrial-scale production and application of immobilized glucose isomerase.** *Methods in Enzymology* 1987, **136**:356–70.
6. Gandhi NN: **Applications of lipase.** *Journal of the American Oil Chemists' Society* 1997, **74**:621–34.
7. Nakamura CE, Whited GM: **Metabolic engineering for the microbial production of 1,3-propanediol.** *Current Opinion in Biotechnology* 2003, **14**:454–9.
8. Bommarius AS, Blum JK, Abrahamson MJ: **Status of protein engineering for biocatalysts: how to design an industrially useful biocatalyst.** *Current Opinion in Chemical Biology* 2011, **15**:194–200.
9. Li S, Yang X, Yang S, Zhu M, Wang X: **Technology prospecting on enzymes: application , marketing and engineering.** *Computational and Structural Biotechnology Journal* 2012, **2**.
10. Behrens GA, Hummel A, Padhi SK, Schätzle S, Bornscheuer UT: **Discovery and protein engineering of biocatalysts for organic synthesis.** *Advanced Synthesis & Catalysis* 2011, **353**:2191–215.
11. Kirk O, Borchert TV, Fuglsang CC: **Industrial enzyme applications.** *Current Opinion in Biotechnology* 2002, **13**:345–51.
12. Aberer W, Han M, Klade M, Seebacher U, Spök A, Wallner K, Witzani H: **Collection of information on enzymes.** *European Commission* 2002.
13. Cherry JR, Fidantsef AL: **Directed evolution of industrial enzymes: an update.** *Current Opinion in Biotechnology* 2003, **14**:438–43.

14. Pessela BCC, Mateo C, Fuentes M, Vian A, Garcia JL, Carrascosa AV, Guisán JM, Fernández-Lafuente R: **The immobilization of a thermophilic β -galactosidase on Sepabeads supports decreases product inhibition.** *Enzyme and Microbial Technology* 2003, **33**:199–205.
15. Hu X, Robin S, O'Connell S, Walsh G, Wall JG: **Engineering of a fungal beta-galactosidase to remove product inhibition by galactose.** *Applied Microbiology and Biotechnology* 2010, **87**:1773–82.
16. Andrić P, Meyer AS, Jensen PA, Dam-Johansen K: **Reactor design for minimizing product inhibition during enzymatic lignocellulose hydrolysis: I. Significance and mechanism of cellobiose and glucose inhibition on cellulolytic enzymes.** *Biotechnology Advances* 2010, **28**:308–24.
17. Fang X, Weintraub NL, Mccaw RB, Hu S, Harmon SD, Rice JB, Hammock BD, Spector AA: **Effect of soluble epoxide hydrolase inhibition on epoxyeicosatrienoic acid metabolism in human blood vessels.** *American Journal of Physiology Heart and Circulatory Physiology* 2004, **52242**:2412–20.
18. Tanaka K, Fukase K, Katsumura S: **New strategy in synthetic biology: from enzyme inhibition and natural products synthesis to PET imaging by 6pi-azaelectrocyclization.** *Chemical Record* 2010, **10**:119–39.
19. Xu D, Li N, He Y, Timofeyev V, Lu L, Tsai H-J, Kim I-H, Tuteja D, Mateo RKP, Singapur A, et al.: **Prevention and reversal of cardiac hypertrophy by soluble epoxide hydrolase inhibitors.** *Proceedings of the National Academy of Sciences of the United States of America* 2006, **103**:18733–8.
20. Locuson CW, Suzuki H, Rettie AE, Jones JP: **Charge and substituent effects on affinity and metabolism of benzbromarone-based CYP2C19 inhibitors.** *Journal of Medicinal Chemistry* 2004, **47**:6768–76.
21. Povolotskaya IS, Kondrashov FA: **Sequence space and the ongoing expansion of the protein universe.** *Nature* 2010, **465**:922–6.
22. Jiang L, Althoff EA, Clemente FR, Doyle L, Röthlisberger D, Zanghellini A, Gallaher JL, Betker JL, Tanaka F, Barbas CF, et al.: **De novo computational design of retro-aldol enzymes.** *Science* 2008, **319**:1387–91.
23. Nanda V, Koder RL: **Designing artificial enzymes by intuition and computation.** *Nature Chemistry* 2010, **2**:15–24.
24. Romero PA, Arnold FH: **Exploring protein fitness landscapes by directed evolution.** *Nature reviews. Molecular Cell Biology* 2009, **10**:866–76.

25. Murakami H, Hohsaka T, Sisido M: **Random insertion and deletion of arbitrary number of bases for codon-based random mutation of DNAs.** *Nature Biotechnology* 2002, **20**:76–81.
26. Tao H, Cornish VW: **Milestones in directed enzyme evolution.** *Current Opinion in Chemical Biology* 2002, **6**:858–64.
27. Chambers I, Frampton J, Goldfarb P, Affara N, Mcbain W, Harrison PR: **The structure of the mouse glutathione peroxidase gene: the Selenocysteine in the active site is encoded by the 'termination'.** *The EMBO Journal* 1986, **5**:1221–7.
28. Zinoni F, Birkmann A, Stadtman TC, Böck A: **Nucleotide sequence and expression of the selenocysteine-containing polypeptide of formate dehydrogenase (formate-hydrogen-lyase-linked) from *Escherichia coli*.** *Proceedings of the National Academy of Sciences of the United States of America* 1986, **83**:4650–4.
29. Bock A, Forchhammer K, Heider J, Leinfelder W, Sawers G, Veprek B, Zinoni F: **MicroReview Selenocysteine: the 21st amino acid.** *Molecular Microbiology* 1991, **5**:515–20.
30. Srinivasan G, James CM, Krzycki JA: **Pyrrolysine encoded by UAG in Archaea: charging of a UAG-decoding specialized tRNA.** *Science* 2002, **296**:1459–62.
31. Budisa N: **Prolegomena to future experimental efforts on genetic code engineering by expanding its amino acid repertoire.** *Angewandte Chemie International Ed.* 2004, **43**:6426–63.
32. Link AJ, Mock ML, Tirrell DA: **Non-canonical amino acids in protein engineering.** *Current Opinion in Biotechnology* 2003, **14**:603–9.
33. Liu CC, Schultz PG: **Adding new chemistries to the genetic code.** *Annual Review of Biochemistry* 2010, **79**:413–44.
34. Johnson JA, Lu YY, Van Deventer JA, Tirrell DA: **Residue-specific incorporation of non-canonical amino acids into proteins: recent developments and applications.** *Current Opinion in Chemical Biology* 2010, **14**:774–80.
35. Tang Y, Tirrell DA: **Attenuation of the editing activity of the *Escherichia coli* leucyl-tRNA synthetase allows incorporation of novel amino acids into proteins *in vivo*.** *Biochemistry* 2002, **41**:10635–45.
36. Wang P, Tang Y, Tirrell DA: **Incorporation of trifluoroisoleucine into proteins *in vivo*.** *Journal of the American Chemical Society* 2003, **125**:6900–6.

37. Langer R, Tirrell DA: **Designing materials for biology and medicine.** *Nature* 2004, **428**:487–92.
38. Schlesinger S, Schlesinger MJ: **The Effect of amino acid analogues on alkaline phosphatase formation in *Escherichia coli* K-12.** *The Journal of Biological Chemistry* 1967, **09226**:3369–72.
39. Schlesinger S, Schlesinger MJ: **The effect of amino acid analogues on alkaline phosphatase formation in *Escherichia coli* K-12.** *The Journal of Biological Chemistry* 1969, **244**:3803–9.
40. Beiboer SH, Van den Berg B, Dekker N, Cox RC, Verheij HM: **Incorporation of an unnatural amino acid in the active site of porcine pancreatic phospholipase A2. Substitution of histidine by 1,2,4-triazole-3-alanine yields an enzyme with high activity at acidic pH.** *Protein Engineering* 1996, **9**:345–52.
41. Soumilion P, Fastrez J: **Incorporation of 1,2,4-triazole-3-alanine into a mutant of phage lambda lysozyme containing a single histidine.** *Protein Engineering* 1998, **11**:213–7.
42. Brooks DJ, Fresco JR, Lesk AM, Singh M: **Evolution of amino acid frequencies in proteins over deep time: inferred order of introduction of amino acids into the genetic code.** *Molecular Biology and Evolution* 2002, **19**:1645–55.
43. Schlesinger S: **The effect of formation of amino acid analogues in *Escherichia coli* K-12 on alkaline phosphatase.** *The Journal of Biological Chemistry* 1968, **243**: 3877-83.
44. Montclare JK, Tirrell DA: **Evolving proteins of novel composition.** *Angewandte Chemie International Ed.* 2006, **45**:4518–21.
45. Yoo TH, Link AJ, Tirrell DA: **Evolution of a fluorinated green fluorescent protein.** *Proceedings of the National Academy of Sciences of the United States of America* 2007, **104**:13887–90.
46. Hoesl MG, Larregola M, Cui H, Budisa N: **Azatriptophans as tools to study polarity requirements for folding of green fluorescent protein.** *Journal of Peptide Science : Sn Official Publication of the European Peptide Society* 2010, **16**:589–95.
47. Armstrong RN: **Structure, catalytic mechanism, and evolution of the glutathione transferases.** *Chemical Research in Toxicology* 1997, **10**:2-18.
48. Yoo J, Bennett M, Schaack J, Rajbhandary UL: **A possible approach to site-specific insertion of two different unnatural amino acids into proteins in mammalian cells via nonsense suppression.** *Chemistry & Biology* 2003, **10**:1095–102.

49. Rodriguez EA, Lester HA, Dougherty DA: ***In vivo* incorporation of multiple unnatural amino acids through nonsense and frameshift suppression.** *Proceedings of the National Academy of Sciences of the United States of America* 2006, **103**:8650–5.
50. Carrico IS, Maskarinec SA, Heilshorn SC, Mock ML, Liu JC, Nowatzki PJ, Franck C, Ravichandran G, Tirrell DA: **Lithographic patterning of photoreactive cell-adhesive proteins.** *Journal of the American Chemical Society* 2007, **129**:4874–5.
51. Cho H, Daniel T, Buechler YJ, Litzinger DC, Maio Z, Putnam A-MH, Kraynov VS, Sim B-C, Bussell S, Javahishvili T, et al.: **Optimized clinical performance of growth hormone with an expanded genetic code.** *Proceedings of the National Academy of Sciences of the United States of America* 2011, **108**:9060–5.
52. Marek P, Mukherjee S, Zanni MT, Raleigh DP: **Residue-specific, real-time characterization of lag-phase species and fibril growth during amyloid formation: a combined fluorescence and IR study of p-cyanophenylalanine analogs of islet amyloid polypeptide.** *Journal of Molecular Biology* 2010, **400**:878–88.
53. Taskent-Sezgin H, Chung J, Patsalo V, Miyake-Stoner SJ, Miller AM, Brewer SH, Mehl RA, Green DF, Raleigh DP, Carrico I: **Interpretation of p-cyanophenylalanine fluorescence in proteins in terms of solvent exposure and contribution of side-chain quenchers: a combined fluorescence, IR and molecular dynamics study.** *Biochemistry* 2009, **48**:9040–6.
54. Taskent-Sezgin H, Marek P, Thomas R, Goldberg D, Chung J, Carrico I, Raleigh DP: **Modulation of p-cyanophenylalanine fluorescence by amino acid side chains and rational design of fluorescence probes of alpha-helix formation.** *Biochemistry* 2010, **49**:6290–5.
55. Jones DH, Cellitti SE, Hao X, Zhang Q, Jahnz M, Summerer D, Schultz PG, Uno T, Geierstanger BH: **Site-specific labeling of proteins with NMR-active unnatural amino acids.** *Journal of Biomolecular NMR* 2010, **46**:89–100.
56. Cellitti SE, Jones DH, Lagpacan L, Hao X, Zhang Q, Hu H, Brittain SM, Brinker A, Caldwell J, Bursulaya B, et al.: ***In vivo* incorporation of unnatural amino acids to probe structure, dynamics, and ligand binding in a large protein by nuclear magnetic resonance spectroscopy.** *Journal of the American Chemical Society* 2008, **130**:9268–81.
57. Hammill JT, Miyake-Stoner S, Hazen JL, Jackson JC, Mehl RA: **Preparation of site-specifically labeled fluorinated proteins for ¹⁹F-NMR structural characterization.** *Nature Protocols* 2007, **2**:2601–7.
58. Holzberger B, Rubini M, Möller HM, Marx A: **A highly active DNA polymerase with a fluorous core.** *Angewandte Chemie International Ed.* 2010, **49**:1324–7.

59. Lepthien S, Merkel L, Budisa N: **In vivo double and triple labeling of proteins using synthetic amino acids.** *Angewandte Chemie International Ed.* 2010, **49**:5446–50.
60. Votchitseva YA, Efremenko EN, Varfolomeyev SD: **Insertion of an unnatural amino acid into the protein structure: preparation and properties of 3-fluorotyrosine containing organophosphate hydrolase.** *Russian Chemical Bulletin* 2006, **55**:369–74.
61. Bae JH, Alefelder S, Kaiser JT, Friedrich R, Moroder L, Huber R, Budisa N: **Incorporation of beta-selenolo[3,2-b]pyrrolyl-alanine into proteins for phase determination in protein X-ray crystallography.** *Journal of Molecular Biology* 2001, **309**:925–36.
62. Kodama K, Nakayama H, Sakamoto K, Fukuzawa S, Kigawa T, Yabuki T, Kitabatake M, Takio K, Yokoyama S: **Site-specific incorporation of 4-iodo-L-phenylalanine through opal suppression.** *Journal of Biochemistry* 2010, **148**:179–87.
63. Sakamoto K, Murayama K, Oki K, Iraha F, Kato-Murayama M, Takahashi M, Ohtake K, Kobayashi T, Kuramitsu S, Shirouzu M, et al.: **Genetic encoding of 3-iodo-L-tyrosine in *Escherichia coli* for single-wavelength anomalous dispersion phasing in protein crystallography.** *Structure* 2009, **17**:335–44.
64. Xie J, Wang L, Wu N, Brock A, Spraggon G, Schultz PG: **The site-specific incorporation of *p*-iodo-L-phenylalanine into proteins for structure determination.** *Nature Biotechnology* 2004, **22**:1297–301.
65. Ealick SE: **Advances in multiple wavelength anomalous diffraction crystallography.** *Current Opinion in Chemical Biology* 2000, **4**:495–9.
66. Walden H: **Selenium incorporation using recombinant techniques.** *Acta Crystallographica Section D, Biological Crystallography* 2010, **66**:352–7.
67. Wang L, Xie J, Deniz AA, Schultz PG: **Unnatural amino acid mutagenesis of green fluorescent protein.** *The Journal of Organic Chemistry* 2003, **68**:174–6.
68. Kwon I, Tirrell DA: **Site-specific incorporation of tryptophan analogues into recombinant proteins in bacterial cells.** *Journal of the American Chemical Society* 2007, **129**:10431–7.
69. Parsons JF, Xiao G, Gilliland GL, Armstrong RN: **Enzymes harboring unnatural amino acids: mechanistic and structural analysis of the enhanced catalytic activity of a glutathione transferase containing 5-fluorotryptophan.** *Biochemistry* 1998, **37**:6286–94.

70. Nastri HG, Evans PD, Walker IH, Riggs PD: **Catalytic and DNA binding properties of PvuII restriction endonuclease mutants.** *The Journal of Biological Chemistry* 1997, **272**:25761–7.
71. Dominguez MA, Thornton KC, Melendez MG, Dupureur CM: **Differential effects of isomeric incorporation of fluorophenylalanines into PvuII endonuclease.** *Proteins* 2001, **45**:55–61.
72. Miura Y, Fulco AJ: **(*w*-2) hydroxylation of fatty acids by a soluble system from *Bacillus megaterium*.** *The Journal of Biological Chemistry* 1974, **249**:1880–8.
73. Cirino PC, Tang Y, Takahashi K, Tirrell DA, Arnold FH: **Global incorporation of norleucine in place of methionine in cytochrome P450 BM-3 heme domain increases peroxygenase activity.** *Biotechnology and Bioengineering* 2003, **83**:729–34.
74. Goerke AR, Loening AM, Gambhir SS, Swartz JR: **Cell-free metabolic engineering promotes high-level production of bioactive *Gaussia princeps* luciferase.** *Metabolic Engineering* 2008, **10**:187–200.
75. Tannous BA, Kim D-E, Fernandez JL, Weissleder R, Breakefield XO: **Codon-optimized *Gaussia* luciferase cDNA for mammalian gene expression in culture and *in vivo*.** *Molecular Therapy: the Journal of the American Society of Gene Therapy* 2005, **11**:435–43.
76. Tannous BA: ***Gaussia* luciferase reporter assay for monitoring biological processes in culture and *in vivo*.** *Nature Protocols* 2009, **4**:582–91.
77. Welsh JP, Patel KG, Manthiram K, Swartz JR: **Multiply mutated *Gaussia* luciferases provide prolonged and intense bioluminescence.** *Biochemical and Biophysical Research Communications* 2009, **389**:563–8.
78. Roth SY, Denu JM, Allis CD: **Histone acetyltransferases.** *Annual Review of Biochemistry* 2001, **70**:81–120.
79. Voloshchuk N, Zhu AY, Snyder D, Montclare JK: **Positional effects of monofluorinated phenylalanines on histone acetyltransferase stability and activity.** *Bioorganic & Medicinal Chemistry Letters* 2009, **19**:5449–51.
80. Holzberger B, Marx A: **Replacing 32 proline residues by a noncanonical amino acid results in a highly active DNA polymerase.** *Journal of the American Chemical Society* 2010, **132**:15708–13.
81. Svendsen A: **Lipase protein engineering.** *Biochimica et Biophysica Acta* 2000, **1543**:223–38.

82. Grove JI, Lovering AL, Guise C, Race PR, Wrighton CJ, White SA, Hyde EI, Searle PF: **Generation of *Escherichia Coli* nitroreductase mutants conferring improved cell sensitization to the prodrug CB1954.** *Cancer Research* 2003, **63**:5532-37.
83. Jackson JC, Duffy SP, Hess KR, Mehl RA: **Improving nature's enzyme active site with genetically encoded unnatural amino acids.** *Journal of the American Chemical Society* 2006, **128**:11124-7.
84. Ugwumba IN, Ozawa K, Xu Z-Q, Ely F, Foo J-L, Herlt AJ, Coppin C, Brown S, Taylor MC, Ollis DL, et al.: **Improving a natural enzyme activity through incorporation of unnatural amino acids.** *Journal of the American Chemical Society* 2011, **133**:326-33.
85. Schnell JR, Dyson HJ, Wright PE: **Structure, dynamics, and catalytic function of dihydrofolate reductase.** *Annual Review of Biophysics and Biomolecular Structure* 2004, **33**:119-40.
86. Cody V, Luft JR, Pangborn W: **Understanding the role of Leu22 variants in methotrexate resistance: comparison of wild-type and Leu22Arg variant mouse and human dihydrofolate reductase ternary crystal complexes with methotrexate and NADPH.** *Acta Crystallographica Section D, Biological Crystallography* 2005, **61**:147-55.
87. Cody V, Pace J, Chisum K, Rosowsky A: **New insights into DHFR interactions: analysis of *pneumocystis carinii* and mouse DHFR complexes with NADPH and two highly potent 5- (w-Carboxy (alkylxy) trimethoprim derivatives reveals conformational correlations with cctivity and novel parallel ring stacking interactions.** *Proteins: Structure, Function, and Bioinformatics* 2006, **65**:959-69.
88. Cody V, Pace J, Piraino J, Queener SF: **Crystallographic analysis reveals a novel second binding site for trimethoprim in active site double mutants of human dihydrofolate reductase.** *Journal of Structural Biology* 2011, **176**:52-9.
89. Volpato JP, Pelletier JN: **Mutational "hot-spots" in mammalian, bacterial and protozoal dihydrofolate reductases associated with antifolate resistance: sequence and structural comparison.** *Drug Resistance Updates: Reviews and Commentaries in Antimicrobial and Anticancer Chemotherapy* 2009, **12**:28-41.
90. Cody V, Pace J, Nowak J: **Structural analysis of human dihydrofolate reductase as a binary complex with the potent and selective inhibitor 2,4-diamino-6-{2'-O-(3-carboxypropyl)oxydibenz[b,f]-azepin-5-yl}methylpteridine reveals an unusual binding mode.** *Acta Crystallographica Section D, Biological Crystallography* 2011, **67**:875-80.
91. Kwon I, Wang P, Tirrell DA: **Design of a bacterial host for site-specific incorporation of *p*-bromophenylalanine into recombinant proteins.** *Journal of the American Chemical Society* 2006, **128**:11778-83.

92. Rajagopalan PTR, Zhang Z, McCourt L, Dwyer M, Benkovic SJ, Hammes GG: **Interaction of dihydrofolate reductase with methotrexate: ensemble and single-molecule kinetics.** *Proceedings of the National Academy of Sciences of the United States of America* 2002, **99**:13481–6.
93. Thillet J, Absil J, Stone SR: **Site-directed mutagenesis of mouse dihydrofolate reductase.** *The Journal of Biological Chemistry* 1988, **263**:12500–8.
94. Gfeller D, Michielin O, Zoete V: **Expanding molecular modeling and design tools to non-natural sidechains.** *Journal of Computational Chemistry* 2012, **33**:1525–35.
95. Schrodinger, PyMOL Molecular Graphics System, Version 1.3r1, LLC, 2010.
96. Beatty KE, Tirrell DA: **Noncanonical amino acids in protein science and engineering.** *Nucleic Acids and Molecular Biology* 2009, **22**:127-53.
97. Waugh DS: **Making the most of affinity tags.** *Trends in Biotechnology* 2005, **23**:316–20.
98. Bollag DM, Rozycki MD, Edelstein SJ: **Protein methods.** 1996, 2nd edition.
99. Rice RH, Means GE, Brown WD: **Stabilization of bovine trypsin by reductive methylation.** *Biochemica et Biophysica Acta* 1977, **492**:316-21.
100. Caprioli RM, Farmer TB, Gile J: **Molecular imaging of biological samples: localization of peptides and proteins using MALDI-TOF MS.** *Analytical Chemistry* 1997, **69**:4751–60.
101. Jurinke C, Oeth P, Boom D: **MALDI-TOF mass spectrometry.** *Molecular Biotechnology* 2004, **26**:147-63.
102. Gill SC, Hippel PH: **Calculation of protein extinction coefficients from amino acid sequence data.** *Analytical Biochemistry* 1989, **182**:319-26.
103. Kane JF, Hartley DL: **Formation of recombinant protein inclusion bodies in *Escherichia coil*.** *Trends in Biotechnology* 1988, **6**:95-101.
104. Mitrack A, King J: **Protein folding intermediates and inclusion body formation.** *Nature Biotechnology* 1987, **7**:690-7.
105. Taira K, Benkovic SJ: **Evaluation of the importance of hydrophobic interactions in drug binding to dihydrofolate reductase.** *Journal of Medicinal Chemistry* 1988, **31**:129–37.
106. Cornish-Bowden A: **Fundamentals of Enzyme Kinetics.** Wiley-Blackwell 2012, 4th edition.